A Conceptual Model of Ocean Heat Uptake under Climate Change

DAVID P. MARSHALL AND LAURE ZANNA

Department of Physics, University of Oxford, Oxford, United Kingdom

ABSTRACT

A conceptual model of ocean heat uptake is developed as a multilayer generalization of Gnanadesikan. The roles of Southern Ocean Ekman and eddy transports, North Atlantic Deep Water (NADW) formation, and diapycnal mixing in controlling ocean stratification and transient heat uptake are investigated under climate change scenarios, including imposed surface warming, increased Southern Ocean wind forcing, with or without eddy compensation, and weakened meridional overturning circulation (MOC) induced by reduced NADW formation. With realistic profiles of diapycnal mixing, ocean heat uptake is dominated by Southern Ocean Ekman transport and its long-term adjustment controlled by the Southern Ocean eddy transport. The time scale of adjustment setting the rate of ocean heat uptake increases with depth. For scenarios with increased Southern Ocean wind forcing or weakened MOC, deepened stratification results in enhanced ocean heat uptake. In each of these experiments, the role of diapycnal mixing in setting ocean stratification and heat uptake is secondary. Conversely, in experiments with enhanced diapycnal mixing as employed in "upwelling diffusion" slab models, the contributions of diapycnal mixing and Southern Ocean Ekman transport to the net heat uptake are comparable, but the stratification extends unrealistically to the sea floor. The simple model is applied to interpret the output of an Earth system model, the Second Generation Canadian Earth System Model (CanESM2), in which the atmospheric CO_2 concentration is increased by 1% yr^{-1} until quadrupling, where it is found that Southern Ocean Ekman transport is essential to reproduce the magnitude and vertical profile of ocean heat uptake.

1. Introduction

The rate of global warming is dictated mainly by the radiative forcing due to the increase of anthropogenic greenhouse gases and the ocean heat uptake (Charney 1979). Recent estimates of the ocean heat uptake have shown that the World Ocean above 2000-m depth has warmed at a rate of 0.39 W m^{-2} since 1950 (Levitus et al. 2012). Therefore, between 80% and 90% of the earth radiation imbalance due to the anthropogenic forcing has been absorbed by the ocean (Levitus et al. 2000, 2005). The rate of warming of the upper ocean is currently larger than that of the deep ocean. The upper ocean heat uptake (above 700 m) is estimated to be around 0.26 W m^{-2} since 1960 (Levitus et al. 2012; Balmaseda et al. 2013) while the ocean heat uptake below 2000 m is estimated to be around 0.1 W m^{-2}, mainly due to the contribution of Antarctic Bottom Water (AABW) formation (Purkey and Johnson 2010). The rate of ocean heat uptake influences not only the rate and the surface pattern of warming but also the rate of global-mean sea level rise due to thermal expansion of seawater on time scales of decades to millennia.

The dynamical processes controlling ocean heat uptake involve an interplay between ocean ventilation, stratification, and the circulation driven by wind and buoyancy forcing. Because of large uncertainties in current observational estimates of ocean heat content, especially at depth, and the limitations of ocean climate models, ocean heat uptake remains a key source of uncertainty in predictions of transient climate change. For example, Boé et al. (2009) identify the deep ocean heat uptake in CMIP3 models to be a major source of spread in simulations of twenty-first-century climate change. The study of Kuhlbrodt and Gregory (2012) suggests that weak ocean stratification in general circulation models (GCMs) results in an overestimate of ocean heat uptake and underestimate of surface warming, with implications for sea level rise estimates.

In the climate community, idealized models are frequently used to understand the mechanisms responsible

Corresponding author address: Dr. David P. Marshall, Department of Physics, Clarendon Laboratory, University of Oxford, Parks Road, Oxford OX1 3PU, United Kingdom.
E-mail: marshall@atm.ox.ac.uk

for the rate of global warming (e.g., Hansen et al. 1985) and interpret results of GCMs. For example, box models can provide some insights into the behavior of the temperature response due to radiative forcing while mimicking the role of ocean heat uptake (e.g., Gregory 2000; Held et al. 2010). Often the ocean is divided in two boxes representing the mixed layer and the deep ocean with the rate of heat uptake being proportional to the temperature difference between the two boxes. In this model, the climate evolves with a fast time scale of a few years and a slow time scale dictated mostly by the ocean heat uptake and the radiative feedbacks. However, the rate of heat uptake varies between GCMs and cannot be easily tied to any physical constraint.

A related approach is to model the ocean as a series of stacked layers in which, following the "abyssal recipe" of Munk (1966), upwelling of cold, dense water formed at high latitudes is balanced by a downward diffusive flux of heat (e.g., Hoffert et al. 1980; Harvey and Schneider 1985; Raper and Cubasch 1996; Raper et al. 2001). The problem with this approach is that the required "effective diffusivity" from diapycnal mixing is generally an order of magnitude larger than values inferred from microstructure (Polzin et al. 1997) and tracer release (Ledwell et al. 1998) measurements in the upper part of the ocean. While enhanced levels of diapycnal mixing have been observed in the abyssal ocean where internal waves scatter off rough bottom topography (Polzin et al. 1997; Naveira Garabato et al. 2004), it is unclear that diapycnal mixing is the dominant process controlling either the mean stratification of the ocean (Wunsch and Ferrari 2004) or its transient heat uptake (e.g., Gregory 2000; Banks and Gregory 2006; Xie and Vallis 2012).

Church et al. (1991) argue that heat penetrates the ocean mostly due to ventilation, similar to a passive tracer, with diapycnal mixing playing a negligible role. However, Banks and Gregory (2006) show using a GCM that heat uptake can vary significantly due to changes in ocean circulation and stratification, and therefore cannot be viewed solely as a passive process. Additionally, several modeling studies have shown that high-latitude regions control the ocean heat uptake in anthropogenic warming scenarios, specifically highlighting the importance of the Southern Ocean processes (e.g., Manabe et al. 1991; Gregory 2000; Huang et al. 2003; Gnanadesikan et al. 2005; Xie and Vallis 2012) and the North Atlantic and its meridional overturning circulation (MOC; e.g., Dalan et al. 2005; Rugenstein et al. 2013).

An alternative model that emphasizes the dynamic role of wind and eddies in the Southern Ocean, North Atlantic Deep Water (NADW) formation as part of the MOC, as well as diapycnal mixing, in maintaining the global pycnocline and the ocean stratification has been developed by Gnanadesikan (1999). In Gnanadesikan's model, the pycnocline is deepened by diapycnal mixing and Southern Ocean Ekman transport, and shallowed by Southern Ocean eddies and NADW formation, thus linking naturally with the sources and sinks of mechanical energy for the global ocean (Munk and Wunsch 1998; Wunsch and Ferrari 2004). However, Gnanadesikan's model consists of just two homogeneous layers and is not well suited to studying ocean heat uptake under transient anthropogenic forcing.

In this paper, our aim is to develop a multilayer generalization of Gnanadesikan (1999) that we hope can replace the "upwelling diffusion" models and simple box models currently used to study ocean heat uptake, both for pedagogical purposes and to analyze the output of coupled ocean–atmosphere GCMs. In particular, we aim to highlight the importance of ocean circulation and associated water-mass transformations, (i.e., "transformations"), as opposed to diapycnal mixing, in controlling ocean stratification, the transient heat uptake, and the vertical heat storage.

An additional aim of the paper is to provide a mechanistic understanding of how the time scale of heat uptake and adjustment varies with the model parameters and as a function of depth. The latter is motivated by the results of Held et al. (2010), building on Hasselmann et al. (1993), that the surface ocean responds to changes in radiative forcing on two distinct time scales: a fast response over a few years within the mixed layer and ventilated upper layers, and a slow "recalcitrant" response associated with the time scale of the deep ocean. Here we show that it is the combination of Southern Ocean eddies and the sensitivity of NADW formation to the stratification that determines the overall time scale of heat uptake and adjustment, consistent with the results of Allison et al. (2011), Jones et al. (2011), and Samelson (2011). Heat uptake over the upper 200 m occurs on a diffusive time scale, below which the adjustment time scale is dominated by Southern Ocean eddies (and the sensitivity of NADW formation to the stratification) with some small contribution from abyssal diapycnal mixing.

The paper is structured as follows. In section 2, the model formulation is described and the parameterization of key processes defined. In section 3 we discuss the vertical structure of the equilibrium stratification in different limits. In section 4 we present and analyze the time-dependent response of the model to imposed surface warming. In section 5 we use the simple model to interpret the results of an Earth System Model under a 1% yr^{-1} CO$_2$ increase scenario. Finally, in section 6 we present a brief concluding discussion of the wider implications of our results.
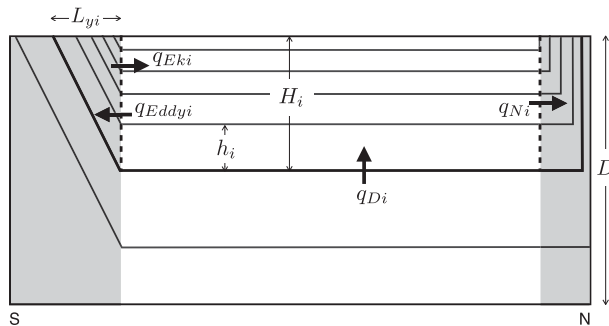
FIG. 1. Schematic of the multilayer extension of the Gnanadesikan ocean model. The model (unshaded region) represents midlatitude stratification north of the ACC, excluding the Southern Ocean and northern high-latitude basins (shaded regions).

2. Model formulation

a. Configuration

The model is an idealized, multilayer extension of that developed by Gnanadesikan (1999) for the global pycnocline, and is sketched schematically in Fig. 1. The ocean is modeled by n layers of Conservative Temperature Θ_i (McDougall 2003) and thickness h_i ($i = 1, 2, \ldots, n$). We define the layer interface depths,

$$H_i = \sum_{j=1}^{i} h_j, \qquad (1)$$

where the total ocean depth is $D = H_n = $ constant. The evolution of each layer interface H_i is controlled by the integrated volume transports into the layers lying above that interface:

$$A \frac{\partial H_i}{\partial t} = q_{\text{Ek}i} - q_{\text{Eddy}i} + q_{Di} - q_{Ni}. \qquad (2)$$

The terms of the right-hand side of (2) represent Southern Ocean Ekman transport, Southern Ocean eddy-induced transport, diapycnal upwelling, and Northern Hemisphere sinking (North Atlantic Deep Water formation) respectively. The evolution of each layer is therefore set by the water mass transformation rates due to each process. The rate at which water is transformed from one Conservative Temperature class to another sets the transformation rate. When there is convergence of water mass transformation in a given layer, then there is a loss of water from that layer; conversely, when there is divergence of water mass transformation in a given layer, then there is a gain of water into that layer. These are referred to as positive and negative water mass formation respectively (Walin 1982; Tziperman 1986). A similar approach is taken in the model of Goodwin (2012) with biogeochemical tracers.

For simplicity, we assume that the lateral area of each layer, A, does not vary significantly between the different layers or with time, and hence can be approximated as constant; this is equivalent to assuming that outcropping of abyssal layers occurs over a relatively small fraction of the surface ocean. Each isopycnal is assumed to have a uniform depth north of the Southern Ocean (Johnson et al. 2007; Allison et al. 2011), due to the efficiency of boundary waves in removing meridional pressure gradients along eastern boundaries (Johnson and Marshall 2002; Marshall and Johnson 2013), as also seen in observations (e.g., Marotzke 1997).

The 1D model describes only the oceans north of the Antarctic Circumpolar Current (ACC), also excluding the northern high-latitude basins and other marginal seas within which the model assumptions are invalid. Therefore the contribution of the northern latitudes is solely via water mass transformation rates. The model shares many common ingredients with that developed by Nikurashin and Vallis (2011) and, in particular, Nikurashin and Vallis (2012), the main difference being that we prescribe scenarios for the rate of NADW formation, as described in section 2f, rather than incorporating a dynamic parameterization. We show in section 4 that incorporating a scaling for NADW as function of the stratification (Gnanadesikan 1999; de Boer et al. 2010a) results in little change in the peak ocean uptake due to the lack of meridional density gradient in the model, but does affect the adjustment time scale.

The model neglects any explicit contributions to ocean heat uptake from salinity variations. In particular, we neglect along-isopycnal eddy mixing, which has been shown to be important for ocean heat uptake in climate models with parameterized ocean eddies (Gregory 2000; note, however, that this study did not employ the Gent and McWilliams parameterization of the eddy bolus velocity). A detailed discussion of the impact of haline forcing on vertical heat transport in the ocean is given by Zika et al. (2013). In our model, haline forcing is included only implicitly to the extent that it controls the NADW formation rates that we prescribe.

We also do not include any explicit representation of AABW formation, which is believed to scale inversely with the strength of Southern Ocean wind forcing as well as being sensitive to air–sea fluxes south of Drake Passage (e.g., Shakespeare and Hogg 2012). Nevertheless, our 1D model does form a realistic amount of AABW [e.g., compared with Lumpkin and Speer (2007)] through a mechanism similar to Ito and Marshall (2008) in which the eddy-induced formation of bottom water is being balanced by diffusive upwelling. AABW is shown to be

a small but increasing contributor to deep ocean uptake (Purkey and Johnson 2010) and its long-term change could affect the overall ocean heat uptake.

b. Conservative Temperature and heat uptake

The use of Conservative Temperature, rather than potential temperature, is because it is better conserved in the ocean interior (Graham and McDougall 2013) and gives a particularly simple expression for the ocean heat content,

$$\mathcal{H} = \rho_0 c_p^0 \Delta\Theta A \sum_{i=1}^{n} H_i, \tag{3}$$

where $\Delta\Theta$ is the temperature difference between each layer, assumed to be constant in this model, ρ_0 is a reference ocean density, and c_p^0 is a constant close to the specific heat capacity at the sea surface of the present ocean (McDougall 2003). Discrepancies between potential temperature and Conservative Temperature occur mostly at high pressure but, over most of the ocean, are small. To allow the time-dependent surface temperature, $\Theta_s(t)$, to vary continuously and yet map smoothly onto the layered structure in the vertical, we introduce an additional variable δ_i that represents the fraction of the ith layer that is outcropped, where $0 \le \delta_i \le 1$. At the sea floor we set $\Theta = \Theta_b$, which we take as constant (but could vary in time).

c. Southern Ocean Ekman transport

The eastward wind stress over the Southern Ocean drives an equatorward ocean Ekman transport, which, in tandem with air–sea heat exchange, represents a cold-to-warm water mass transformation. We specify the magnitude of the Southern Ocean Ekman transport as

$$q_{\mathrm{Ek0}} = \frac{\tau_s L_x}{\rho_0 |f_{\mathrm{ACC}}|} \quad (i \neq n), \tag{4}$$

where τ_s is the zonal wind stress, f_{ACC} is the Coriolis parameter, and L_x is the zonal extent of the Southern Ocean.

We deposit the Ekman transport linearly within the warmest $\Delta\Theta_{\mathrm{Ek}}$ Conservative Temperature class of the model, motivated by the fact that the Ekman transport varies with latitude, resulting in Ekman pumping across a range of Conservative Temperatures. This is compensated by a poleward geostrophic return flow beneath the depth of the Drake Passage, H_{Drake}, where the topography is able to support a zonal pressure gradient, leading to a reduction in the Ekman transformation in the coldest temperature classes. Thus the Ekman transport above the ith interface, taking into account the return geostrophic flow, is prescribed as

$$q_{\mathrm{Ek}i} = \begin{cases} q_{\mathrm{Ek0}} \left(\dfrac{\Theta_s - \Theta_i}{\Delta\Theta_{\mathrm{Ek}}} \right) & (\Theta_i > \Theta_s - \Delta\Theta_{\mathrm{Ek}}), \\[3mm] q_{\mathrm{Ek0}} & (\Theta_i \le \Theta_s - \Delta\Theta_{\mathrm{Ek}}, \quad H_i \le H_{\mathrm{Drake}}), \\[3mm] q_{\mathrm{Ek0}} \left(\dfrac{D - H_i}{D - H_{\mathrm{Drake}}} \right) & (H_i > H_{\mathrm{Drake}}). \end{cases} \tag{5}$$

In the above, we have assumed that the temperature surface $\Theta_s - \Delta\Theta_{\mathrm{Ek}}$ lies above the depth of Drake Passage, H_{Drake}, as is the case for all the solutions presented here.

d. Southern Ocean eddy-induced transport

For the Southern Ocean eddy-induced transport, we adopt the Gent and McWilliams (1990) eddy closure in which eddies extracts potential energy from the background state through an eddy-induced circulation mimicking the effects of baroclinic instability. The form of Gent and McWilliams used is similar to Gnanadesikan (1999) but extended to multiple layers, and tapered beneath Drake Passage in the same manner as for the Ekman term (5) to satisfy the lower boundary condition:

$$q_{\mathrm{Eddy}i} = \begin{cases} -\kappa_{\mathrm{GM}} L_x \dfrac{H_i}{L_{yi}} & (H_i \le H_{\mathrm{Drake}}), \\[3mm] -\kappa_{\mathrm{GM}} L_x \dfrac{H_i}{L_{yi}} \left(\dfrac{D - H_i}{D - H_{\mathrm{Drake}}} \right) & (H_i > H_{\mathrm{Drake}}). \end{cases} \tag{6}$$

Here L_{yi} is the mean distance between the northernmost extent of the ACC and the outcrop of that isopycnal layer. For simplicity, we assume a linear variation in surface temperature across the ACC and set

$$L_{yi} = L_{y0} \left(\frac{\Theta_i - \Theta_b}{\Theta_s - \Theta_b} \right), \tag{7}$$

where L_{y0} is the mean width the ACC. Note that the latter is broader than the width of Drake Passage due to

the fanning out of the ACC at other longitudes (Allison et al. 2010). The net Southern Ocean transformation is thus a residual between the Ekman and eddy-induced components, $q_{Ek} - q_{Eddy}$ (Marshall 1997; Marshall and Radko 2003).

e. Diapycnal upwelling

We can obtain a simple expression for the diapycnal upwelling across each layer interface through a simple one-dimensional balance between diapycnal advection and diapycnal diffusion:

$$w* \frac{\partial \Theta}{\partial z} = \frac{\partial}{\partial z}\left(\kappa_v \frac{\partial \Theta}{\partial z}\right), \tag{8}$$

where $w*$ is the diapycnal velocity, Θ is Conservative Temperature, and κ_v is the diapycnal diffusivity (Munk 1966).

Taking the Conservative Temperature difference between each layer to be identical, the finite-difference version of (8) is

$$q_{Di} = Aw_i^* = A\left(\frac{\delta_i \kappa_{vi}}{h_i} - \frac{\kappa_{vi+1}}{h_{i+1}}\right). \tag{9}$$

This corresponds to the simplest limit of the more general formula derived by McDougall and Dewar (1998). Physically (9) is intuitive: a thicker layer will surrender fluid to an adjacent thinner layer, given equal variations in Conservative Temperature across each layer. To allow for surface outcropping, the first term includes a contribution from δ_i, the fraction of the layer outcropped. The latter is imposed through the surface boundary conditions, as discussed in section 2b and $\delta_i = 1$ in all layers except that closest to the sea surface. At both the upper and lower boundaries, q_D is set to zero corresponding to a no-flux condition.

The vertical diffusivity κ_{vi} takes two forms in the model, either as a constant independent of depth, or as a vertical profile that depends on the vertical coordinates following Bryan and Lewis (1979) such that

$$\kappa_{vi} = \frac{\kappa_b + \kappa_s}{2} + \frac{\kappa_b - \kappa_s}{\pi}\tan^{-1}\left(\frac{h_i - h_{bl}}{\Delta h_{bl}}\right), \tag{10}$$

where κ_s is the asymptotic value of the surface diffusivity, κ_b is the asymptotic value of the abyssal diffusivity, and the parameters Δh_{bl} and h_{bl} set the shape of the diffusivity profile as function of depth.

f. NADW formation

Finally, we need to prescribe the rate at which water is transformed to North Atlantic Deep Water at northern high latitudes. Gnanadesikan (1999) argues that the rate

of NADW formation should scale as the square of the pycnocline depth, although, as noted by de Boer et al. (2010a) and Fürst and Levermann (2012), there are reasons to question the robustness of such a scaling. These issues are far more complicated in a multilayer model and hence we simply prescribe q_{Ni} for each layer:

$$q_{Ni} = \begin{cases} q_{N0}\sin\left(\dfrac{\pi}{2}\dfrac{\Theta_s - \Theta_i}{\Theta_s - \Theta_N}\right) & (\Theta_i \geq \Theta_N), \\[2ex] q_{N0}\cos^2\left(\dfrac{\pi}{2}\dfrac{\Theta_N - \Theta_i}{\Theta_N - \Theta_A}\right) & (\Theta_N > \Theta_i \geq \Theta_A), \\[2ex] 0 & (\Theta_A > \Theta_i). \end{cases} \tag{11}$$

Here Θ_N is the Conservative Temperature of maximum northern overturning (the upper limit of NADW formation) and Θ_A is the Conservative Temperature at which northern overturning vanishes (the lower limit of NADW formation). An alternative, dynamic closure for q_{Ni} is considered in section 4b.

g. Method of solution

The stratification is modeled through $n = 100$ layers with Conservative Temperatures between $\Theta_b = 1.5°C$ (except in section 5 where $\Theta_b = 0°C$) and $\Theta_s = 25°C$. The prognostic Eq. (2) is time-stepped using a third-order Adams–Bashforth scheme (Durran 1991) with a typical time step of 8×10^4 s, reduced where necessary in order to preserve numerical stability. To prevent division by zero in the calculation of q_{Di}, a minimum layer thickness of 10^{-2} m is imposed in the denominator of (9); the solutions presented are not sensitive to the precise value of this minimum layer thickness. In the limit of finite layers, the piecewise nature of stratification can result in jumps in ocean heat uptake as new layers appear; however, this appears to have no discernible effect on other aspects of the model solutions.

We also set the depth of Drake Passage, $H_{Drake} = 4 \times 10^3$ m, the total ocean depth, $H = 5 \times 10^3$ m, the zonal extent of the Southern Ocean, $L_x = 2 \times 10^7$ m, and the mean width of the ACC, $L_{y0} = 1.5 \times 10^6$ m. The surface area is set to $A = 2 \times 10^{14}$ m, accounting for the ocean surface north of the ACC and excluding the northern high-latitude basins and marginal seas. Details of the remaining parameters are given with each experiment.

3. Equilibrium solutions

Before discussing the transient response of the model and ocean heat uptake to anthropogenic forcing, it is instructive to consider how the equilibrium stratification profile varies as the model parameters and forcing are varied. For the purpose of this section, we define our
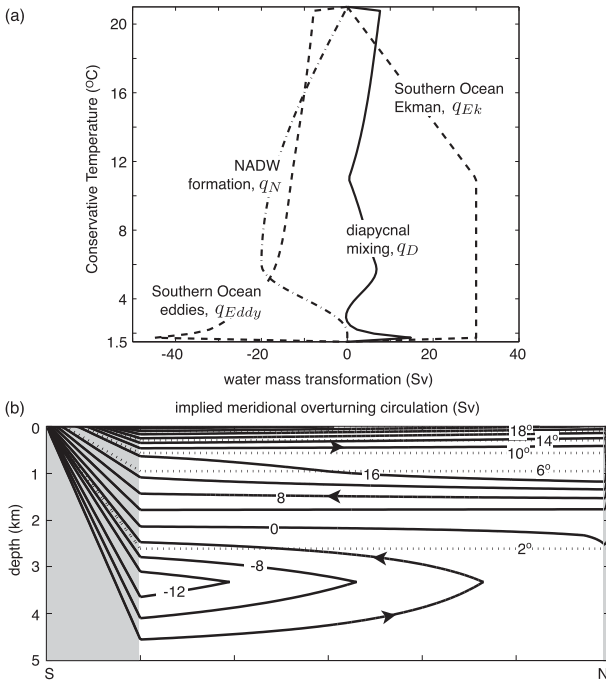
FIG. 2. (a) Water mass transformation due to Southern Ocean Ekman transport, Southern Ocean eddy transport, NADW formation, and diapycnal mixing as function of Conservative Temperature. (b) Implied meridional overturning circulation (solid lines, contour interval of 4 Sv) and Conservative Temperature surfaces (dotted lines, contour interval of 4°C). The shaded regions to the south and north schematically represent the Southern Ocean and high-latitude northern basins over which the 1D model does not apply.
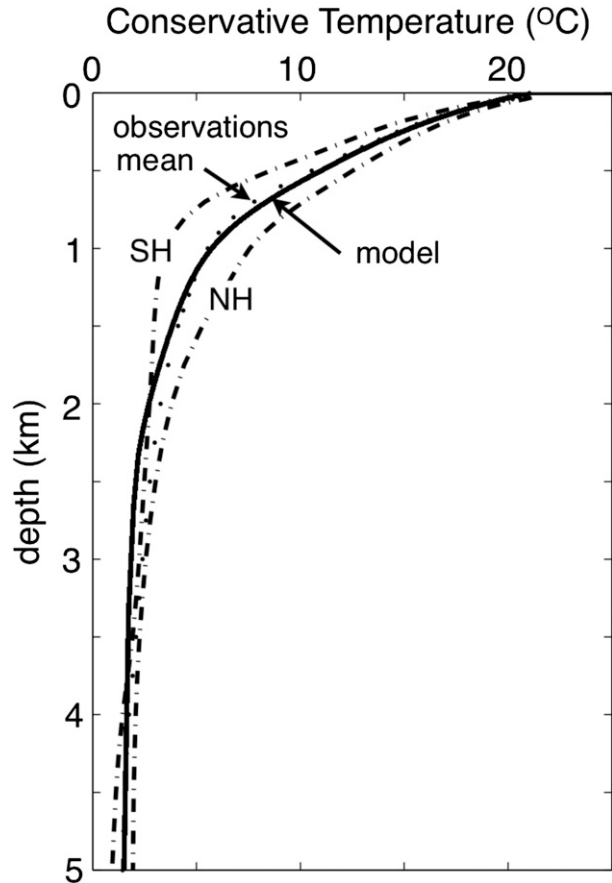

FIG. 3. Equilibrium stratification for the control solution of the 1D model (solid line) compared to observed profiles of Conservative Temperature in the Atlantic. The profiles (dashed–dotted lines) for the Northern Hemisphere (NH) and Southern Hemisphere (SH) are computed between latitudes of 20° and 40° in each hemisphere. The averaged observed profile, taken as the mean between the two hemispheres, is also shown (dotted line).

"control" solution as one with the parameter values: $\kappa_{GM} = 1 \times 10^3 \, \text{m}^2 \, \text{s}^{-1}$, $q_{Ek0} = 30 \, \text{Sv}$ ($1 \, \text{Sv} \equiv 10^6 \, \text{m}^3 \, \text{s}^{-1}$; corresponding to a wind stress of about $0.15 \, \text{N} \, \text{m}^{-2}$ for $f_{ACC} = -1 \times 10^{-4} \, \text{s}^{-1}$), and $q_{N0} = 20 \, \text{Sv}$. The Southern Ocean Ekman transport is deposited in the warmest $\Delta\Theta_{Ek} = 10°\text{C}$ Conservative Temperature class, NADW is formed in the Conservative Temperature range $\{\Theta_A - \Theta_N\} = \{2° - 6°\text{C}\}$, and the surface temperature is $\Theta_s = 21°\text{C}$. The vertical diffusivity is prescribed using the Bryan–Lewis profile (10) with $\kappa_s = 1 \times 10^{-5} \, \text{m}^2 \, \text{s}^{-1}$, $\kappa_b = 1 \times 10^{-4} \, \text{m}^2 \, \text{s}^{-1}$, $\Delta h_{bl} = 0.22 \times 10^3 \, \text{m}$, and $h_{bl} = 2500 \, \text{m}$. In each calculation, the model has been integrated for 10 000 years, after which the surface heat uptake is typically reduced to a magnitude of $10^{-5} \, \text{W} \, \text{m}^{-2}$.

Variations of the four water mass transformation processes with Conservative Temperature in the control integration are plotted in Fig. 2a. The Southern Ocean Ekman transport, q_{Ek} is mostly balanced by a combination of Southern Ocean eddies, q_{Eddy}, and NADW formation, q_N, with the former dominating in Conservative Temperature classes colder than NADW by construction. Diapycnal diffusion is a smaller term at most depths, transforming cold water into warmer water, but is

dominant at the very warmest Conservative Temperatures near the surface and also plays a substantial role in the coldest Conservative Temperature classes corresponding to AABW formation as previously described. While the model stratification is one-dimensional, it is possible to infer the implied two-dimensional MOC by continuity, shown in Fig. 2b. We obtain two cells: over the upper 2–3 km a quasi-adiabatic pole-to-pole NADW cell (cf. Wolfe and Cessi 2011) with an imposed strength of 20 Sv, and over the lower 2–3 km a diffusively driven AABW cell of 15 Sv that forms dynamically through the mechanism described in Ito and Marshall (2008).The structure of the model's MOC compares remarkably well with the observation-derived estimate of the global MOC in Lumpkin and Speer (2007, their Fig. 2).

The equilibrium Conservative Temperature profile in the control solution is compared to climatological observations in Fig. 3, where the latter have been evaluated
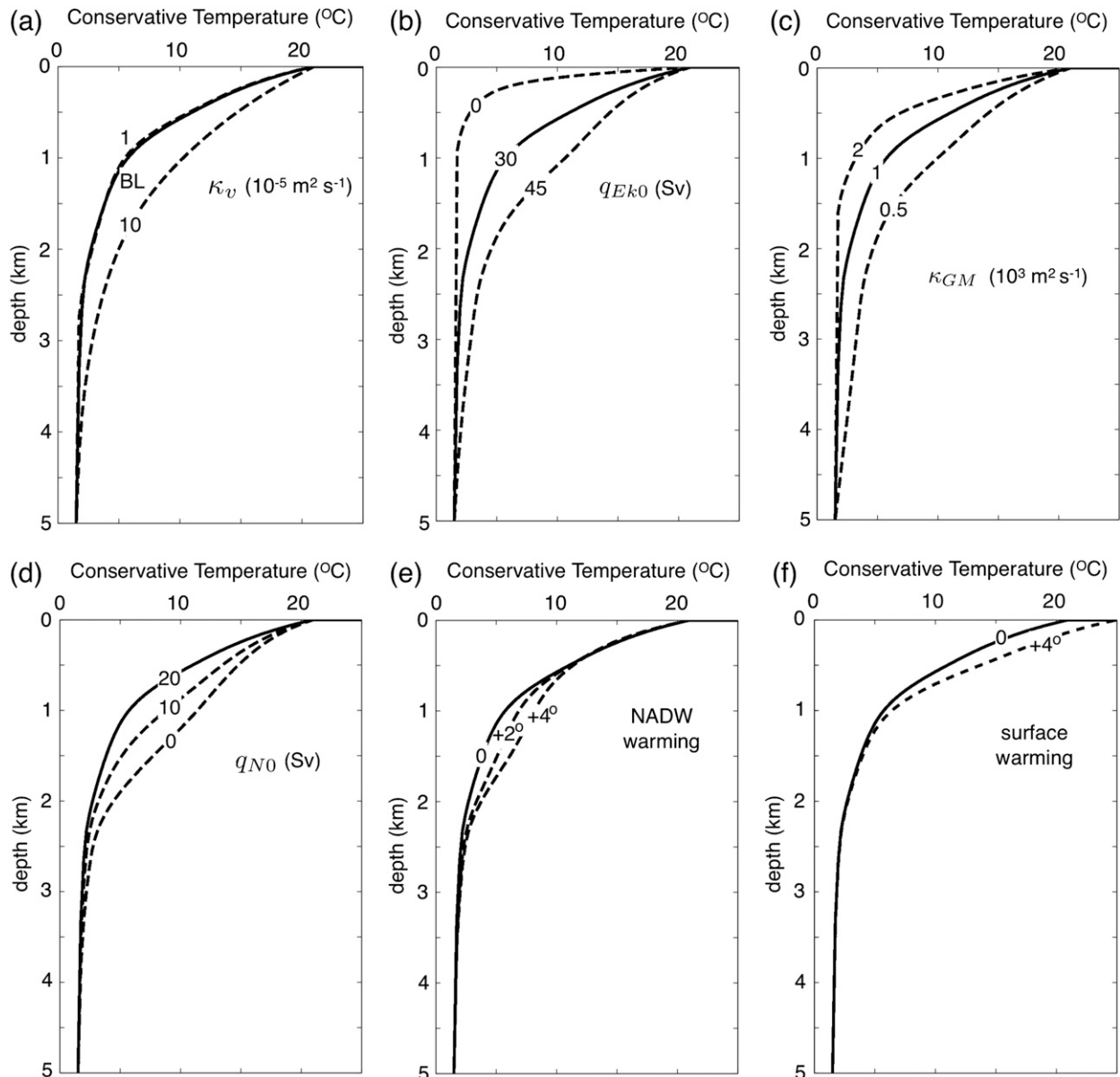
FIG. 4. Sensitivity of equilibrium stratification to different parameters and forcing: (a) diapycnal diffusivity, (b) Southern Ocean Ekman transport, (c) Southern Ocean eddy diffusivity, (d) NADW formation rate, (e) NADW temperature, and (f) surface warming.

using the dataset of Gouretski and Kolterman (2004) and the TEOS-10 toolbox of McDougall and Barker (2011). The solid curve is from the control solution of the 1D model, the dashed curves have been calculated by averaging the climatological data within 40°–20°S and 20°–40°N in the Atlantic (SH and NH respectively), and the dotted curve is the mean of the two hemispheric curves (i.e., excluding the tropics since the tropical thermocline is not represented in the 1D model). Atlantic profiles are chosen for this comparison because 1) the majority of the anthropogenic heat uptake occurs in the Atlantic sector (e.g., in the climate model discussed in

section 5), and 2) salinity variations are greatest in the Atlantic, allowing a crude estimation of the error introduced by neglecting salinity variations in the 1D model.

The 1D model adequately captures the observed vertical Conservative Temperature profile from observations, with slightly warmer Conservative Temperatures between 0.5 and 1 km, and weaker stratification at depth; on the other hand, the abyssal stratification agrees better with observed values in the Pacific (not shown). The effect of varying different parameters on the vertical Conservative Temperature profile is shown in Fig. 4; these are now discussed in the following sections.

a. Diapycnal diffusivity

The effect of replacing the Bryan–Lewis diapycnal diffusion profile with constant diapycnal diffusivities of $\kappa_v = 1 \times 10^{-5}\,\mathrm{m^2\,s^{-1}}$ and $1 \times 10^{-4}\,\mathrm{m^2\,s^{-1}}$ is shown in Fig. 4a. The most striking result is that the enhanced diapycnal diffusion at depth in the Bryan–Lewis profile has remarkably little impact on the stratification at any depth. In contrast, applying enhanced diffusion ($\kappa_v = 1 \times 10^{-4}\,\mathrm{m^2\,s^{-1}}$) over the entire water column leads to a much deeper stratification and excessive warmth at all depths, consistent with the ideas of Sandström (1916) and Munk (1966).

For extremely low values of diapycnal diffusion ($\kappa_v = 10^{-6}\,\mathrm{m^2\,s^{-1}}$ at all depths), the stratification becomes concentrated unrealistically in two internal pycnoclines, above and below the depths of NADW formation (not shown), as previously obtained in an idealized GCM by Vallis (2000); also see Samelson and Vallis (1997).

b. Southern Ocean winds

Southern Ocean wind forcing is the dominant source of mechanical energy for the global ocean (Wunsch and Ferrari 2004) and hence has a substantial impact on the vertical stratification profile and vertical heat transport (e.g., Gnanadesikan et al. 2005). With the Southern Ocean Ekman transport set to zero, the stratification is confined entirely to the upper 700 m and is determined by a Munk (1966)-type balance between the NADW formation and diapycnal upwelling (Fig. 4b). Since the control value of diapycnal diffusion is weak over the upper ocean, consistent with observations, the resultant stratification is confined to a thin, diffusive surface boundary layer (Sandström 1916). Southern Ocean eddies play only a secondary role in this limit since the pycnocline is shallow. In contrast, if the surface Ekman transport is increased to 30 Sv, the pycnocline deepens and extends to below 3 km, now largely opposed by the Southern Ocean eddy bolus transport, but also by NADW formation (Fig. 2a). Further increase in the Ekman transport, to a value of 45 Sv, results in the stratification extending to the sea floor. These results are consistent with a number of recent studies, including Wolfe and Cessi (2010), Nikurashin and Vallis (2011), Radko and Kamenkovich (2011), Kamenkovich and Radko (2011), and Nikurashin and Vallis (2012).

c. Southern Ocean eddies

One of the most critical parameters is the Southern Ocean geostrophic eddy diffusivity, κ_{GM}, set to $1 \times 10^3\,\mathrm{m^2\,s^{-1}}$ in the control integration (Fig. 4c). The role of Southern Ocean eddies is most easily understood if we first neglect

NADW formation such that there is a leading-order compensation between the Southern Ocean Ekman and eddy-induced overturning cells (Danabasoglu et al. 1994). Setting $q_{\mathrm{Eddy}i}$ = constant in (6) shows that the depth of the isopycnals, H_i, varies inversely with the Southern Ocean eddy diffusivity κ_{GM}. Finite NADW formation breaks this simple inverse relation, but nevertheless the basic sensitivity remains. Thus when $\kappa_{\mathrm{GM}} = 2 \times 10^3\,\mathrm{m^2\,s^{-1}}$ the stratification is confined to the upper 1.7 km; in contrast, when $\kappa_{\mathrm{GM}} = 0.5 \times 10^3\,\mathrm{m^2\,s^{-1}}$ the stratification extends to the sea floor. Again, these results are consistent with recent studies, including Wolfe and Cessi (2010), Nikurashin and Vallis (2011), Radko and Kamenkovich (2011), Kamenkovich and Radko (2011), and Nikurashin and Vallis (2012).

d. NADW formation rate and temperature range

NADW formation acts as a sink of warm surface water and a source of relatively cool middepth water, inducing upwelling over the upper 2.5–3 km of the fluid column for the control model parameters. Therefore the effect of halving and removing the NADW formation rate (Fig. 4d) is to deepen the stratification over the upper 3 km. In the limit in which NADW is turned off, the stratification of the upper 3 km becomes close to linear: this is a consequence of the near cancellation of the Southern Ocean Ekman and eddy-induced overturning cells and hence the linear variation of the surface temperature across the Southern Ocean in the model being mapped onto a linear vertical stratification. In reality, the latter result will depend on both the surface temperature gradients and the variation of the eddy diffusivity, κ_{GM}, with the stratification. Similar results are discussed in Wolfe and Cessi (2010) and Nikurashin and Vallis (2012).

The stratification profile is sensitive not only to the NADW formation rate, but also the Conservative Temperature range in which NADW is formed (cf. Wolfe and Cessi 2010, their Fig. 1b). Warmer NADW confines that part of the upwelling balancing NADW formation to warmer Conservative Temperature classes; hence the stratification increases over the Conservative Temperature classes in which NADW is no longer formed (Fig. 4e).

e. Surface temperature

Finally, the effect of increasing the surface temperature by 4°C is shown in Fig. 4f. Basically, the stratification profile has a similar shape but scaled up to satisfy the new surface boundary condition. Note that the heat content anomaly is mostly, but not exclusively, confined to the upper kilometer, in contrast to the heat content anomalies induced by changes in Southern Ocean winds (Fig. 4b),
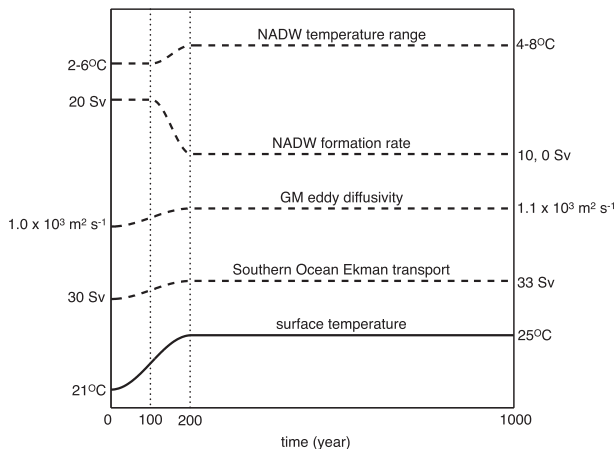
FIG. 5. Forcing anomaly profiles as function of time.

eddies (Fig. 4c), and NADW formation (Figs. 4d,e). Also note that the heat content changes associated with plausible perturbations to Southern Ocean winds and/or eddies or NADW formation are potentially of similar magnitude to those due to the direct effect of the warmer surface boundary conditions.

4. Anthropogenic climate change scenarios

We now present solutions for a range of different anthropogenic climate change scenarios. The aim of these calculations is to quantify the magnitude of plausible variations in the key processes in response to anthropogenic climate forcing, namely surface warming, increase in wind and eddy circulation in the Southern Ocean and MOC weakening. Thus, for each such parameter, $F(t)$, we prescribe

$$F(t) = F_0 + \Delta F \times \begin{cases} 0 & (t < t_1), \\ \sin^2\left(\dfrac{\pi}{2}\dfrac{t - t_1}{t_2 - t_1}\right) & (t_1 \le t \le t_2), \\ 1 & (t_2 < t), \end{cases}$$
(12)

where the change ΔF in F occurs smoothly over the time interval $t_1 \le t \le t_2$. The parameters we vary are plotted in Fig. 5. The surface temperature is increased by 4° over a time interval of 200 yr in each of the scenarios (except for one sensitivity calculation with a 2° warming). In addition, we consider the impact of the Southern Ocean Ekman transport increasing by 10% over the same period, accompanied, or not, by an equivalent increase in the Southern Ocean eddy diffusivity. And finally we consider the impact of NADW formation (or MOC) weakening by 50% and 100% between years 100 and 200, the former

also in conjunction with 2°C warming of the NADW formation Conservative Temperature class. Each of these scenarios is initialized with the control equilibrium solution and integrated for a total of 1000 years.

a. Control scenario forced by surface warming

First we consider a scenario in which only the surface temperature is increased by 4°C over the first 200 years, consistent with estimated projections of temperature increase from preindustrial value under the representative concentration pathway (RCP) 6.0 scenario by year 2200 or Special Report on Emissions Scenarios (SRES) scenario A2 by year 2100 (Rogelj et al. 2012). Plotted in Fig. 6 is the net ocean heat uptake and its vertical partitioning in the depth ranges 0–0.7, 0.7–2, and 2–5 km (Fig. 6a), the ocean Conservative Temperature anomaly at different depths as a function of time (Fig. 6b), and the ocean heat uptake anomaly (Fig. 6c). The latter also shows the heat uptake anomaly due to each of the four processes: Ekman transport, Southern Ocean eddies, NADW formation, and diapycnal diffusion. Note that the heat uptakes are normalized by the surface area of Earth.

The global heat uptake reaches a maximum value of 0.6 W m^{-2} after 150 years before its eventual decay. Relatively little heat uptake occurs through diapycnal diffusion although it does play a proportionately greater role during the initial 100 years of the integration. Instead, by far the largest source of heat uptake is the Southern Ocean Ekman transport. Given that the global stratification is largely controlled by Southern Ocean winds, as discussed by Wolfe and Cessi (2010), Nikurashin and Vallis (2011), Radko and Kamenkovich (2011), Kamenkovich and Radko (2011), and Nikurashin and Vallis (2012), global ocean heat uptake is also largely determined by Southern Ocean Ekman transport (also see Gnanadesikan et al. 2005), especially on short time scales. Physically, this corresponds to Ekman pumping of the surface heat anomaly into the ocean interior.

NADW formation opposes the Ekman heat uptake, essentially because warmer water is now transformed to NADW, therefore representing a net sink of heat. The heat uptake due to Southern Ocean eddies is initially weak and slightly positive before becoming negative and slightly larger than the NADW contribution on the centennial time scale. On short times scales, the eddy heat uptake is dominated by eddy-induced downwelling of warmer water over the Southern Ocean, but on longer time scales the eddy overturning circulation itself adjusts to the changes in stratification dominating the eddy heat uptake. Similar results are obtained if the surface warming anomaly is only 2°C over 200 years instead of 4°C (Fig. 6d); the heat uptake and the contribution from
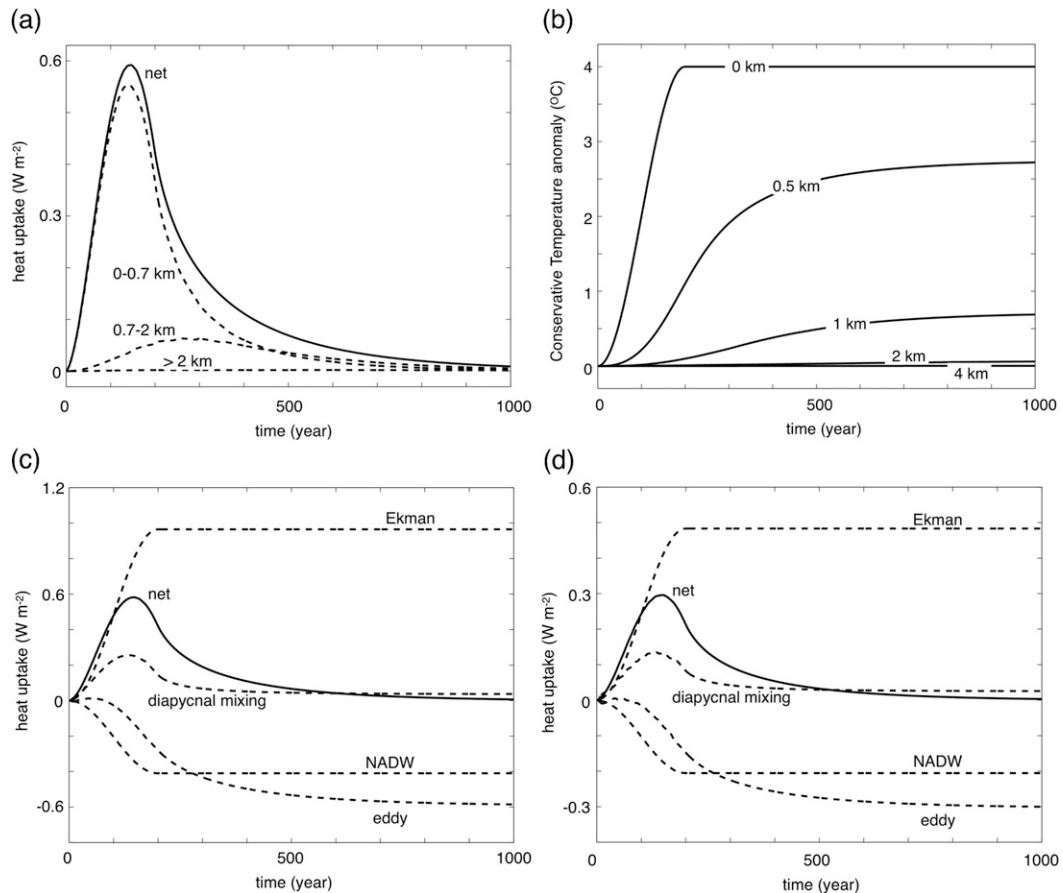
FIG. 6. Control solution with imposed anthropogenic surface warming of 4°C and Bryan–Lewis diapycnal mixing, $\kappa_s = 1 \times 10^{-5} \, \mathrm{m^2 \, s^{-1}}$ and $\kappa_b = 1 \times 10^{-4} \, \mathrm{m^2 \, s^{-1}}$. (a) Net ocean heat uptake and its partitioning over different depth ranges, normalized by the surface area of Earth. (b) Temperature anomaly at different depths as function of time. (c) Net ocean heat uptake and the heat uptake due to the four processes, normalized by the surface area of Earth. (d) As in (c), but with surface warming of only 2°C.

the four dynamical controls scale almost linearly with the applied warming.

The anomalous heat in the ocean is concentrated in the upper 2 km, and in particular over the upper 0.7 km (Figs. 6a,b). Both the upper and midocean heat uptakes, similar to the global heat uptake, are dominated by the Southern Ocean Ekman transport, with smaller contributions from Southern Ocean eddies and NADW formation (not shown). The uptake due to Southern Ocean eddies adjusts most slowly and sets the overall adjustment time-scale, as discussed in the following section. Middepth and abyssal layers are still warming at the end of the simulation, similar to global climate models (Li et al. 2013), with the ocean uptake between 0.7 and 2 km reaching a maximum value of 0.06 W m^{-2} at around 280 yr.

b. Variation of adjustment time scale with depth

The response of the ocean at the surface is determined by the rate at which energy is absorbed at the sea surface (the

net ocean heat uptake) but also by the transformation rates from the surface to the interior. Figures 6a–c show that the ocean equilibrates over many centuries and, indeed, is not fully equilibrated at the end of the 1000-yr integration.

To investigate the adjustment time scales further, in Fig. 7a we show the response of the model to a 1°C surface temperature anomaly applied instantaneously as a step function. The upper 50 m and 100 m adjust on time scales of 30 to 40 years, longer than the time scale of a few years one would expect in the surface mixed layer (e.g., Held et al. 2010), simply reflecting the absence of a surface mixed layer in the model. The more interesting time scales are 200 years at about 500 m, 1000 years at about 1-km depth, and 2000 years in the abyss.

The overall adjustment time scales are controlled by diapycnal mixing and Southern Ocean eddies, as sketched schematically in Fig. 7b, since the Southern
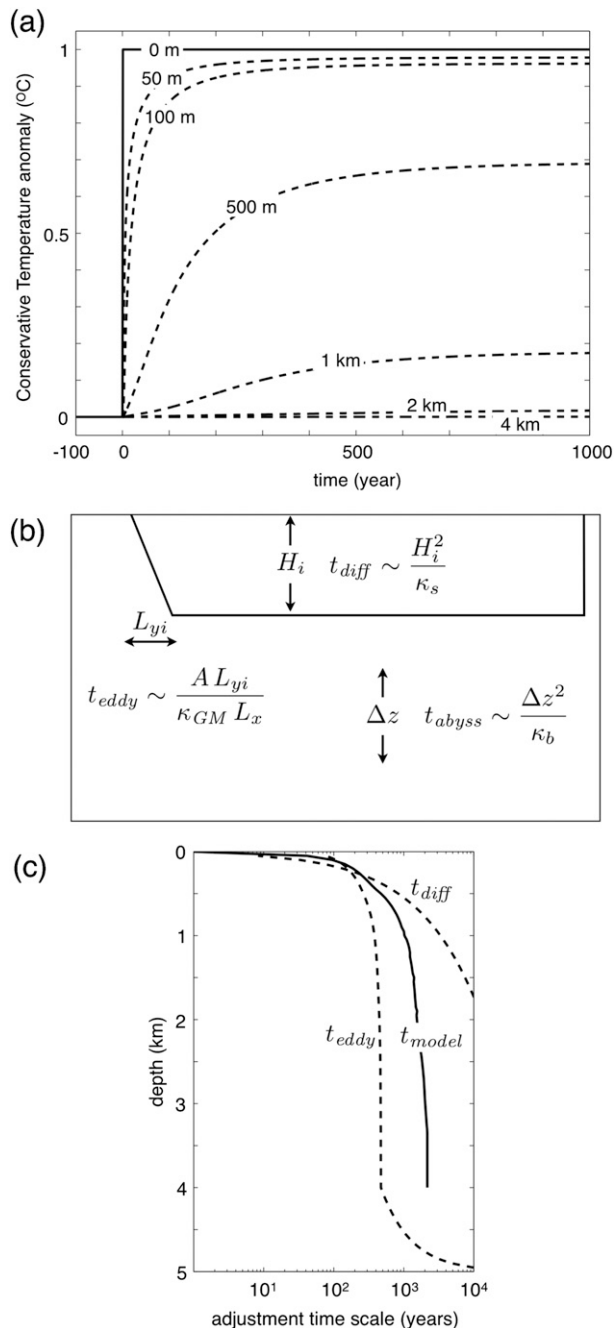
FIG. 7. (a) Conservative Temperature anomalies at different depths under an impulsive (step) surface forcing of 1°C. (b) Schematic illustrating the three pertinent adjustment time scales, t_{diff}, t_{eddy}, and t_{abyss}, as discussed in the main text. (c) Variation of t_{diff} and t_{eddy} with depth, along with an estimate of the adjustment time scale in the model, obtained by fitting an exponential.

Ocean Ekman transport and NADW formation are essentially constant in time. The three pertinent time scales are involved: 1) upper ocean diffusion, 2) Southern Ocean eddies, and 3) abyssal ocean mixing. The surface

temperature anomaly will spread into the interior on the diffusive time scale

$$t_{\mathrm{diff}} \sim \frac{H_i^2}{\kappa_s}, \tag{13}$$

which increases rapidly with depth. Southern Ocean eddies act as a damping on layer depth anomalies on the eddy time scale

$$t_{\mathrm{eddy}} \sim \frac{A L_{yi}}{\kappa_{\mathrm{GM}} L_x}, \tag{14}$$

which increases with depth due to the increasing distance over which the layer slopes in the Southern Ocean, L_{yi}. Finally, enhanced mixing in the abyssal ocean also plays a role in the adjustment on the abyssal diffusive time scale

$$t_{\mathrm{abyss}} \sim \frac{\Delta z^2}{\kappa_b}, \tag{15}$$

where Δz is a typical vertical scale in the abyss (say, 1–2 km).

The diffusive and eddy time scales, t_{diff} and t_{eddy}, are plotted in Fig. 7c as a function of depth, along with a best estimate of the adjustment time scale by fitting an exponential curve. There is at least a factor of 2 uncertainty in the latter at depths below about 1 km, depending on the precise details of how the fit is performed (not shown); nevertheless the plotted curve gives a qualitative idea of how the adjustment time scale varies with depth. The abyssal diffusive time scale, t_{abyss}, is on the order of 10^3 years, assuming a vertical scale of about 2 km. The diffusive time scale dominates over the upper 200 m. However, at deeper levels, the adjustment appears to be set mostly by Southern Ocean eddy time scale, consistent with the analyses of the time-dependent two-layer Gnanadesikan and related models in Allison et al. (2011), Jones et al. (2011), and Samelson (2011); however, the overall adjustment time scale is slightly increased due to the role of the abyssal diapycnal mixing in establishing the equilibrated abyssal stratification. Note, that in contrast to the two-layer models of Held et al. (2010) and Geoffroy et al. (2013a), a continuous spectrum of time scales is obtained as a function of depth, which are readily understood in terms of the variation of eddy time scale with depth in the continuous 1D model.

c. Overall adjustment time scale

While diapycnal mixing sets the adjustment time scale over the upper 200 m, since the heat uptake occurs over a much greater depth range, the overall adjustment should be controlled by the parameterization of Southern

Ocean eddies, as found in Allison et al. (2011), Jones et al. (2011), and Samelson (2011), and consistent with Fig. 6c, where the eddy component of the heat uptake is the slowest to equilibrate. This is confirmed in Fig. 8a where we compare the heat uptake anomaly of the control integration (as in Fig. 6c) with cases in which the Southern Ocean eddy diffusivity is increased and decreased by a factor of 2.

In the cases considered thus far, the NADW formation is independent of the pycnocline depth. However, Jones et al. (2011) and Allison et al. (2011) have shown that the adjustment time scale is also affected by the sensitivity of the NADW formation rate to the pycnocline depth in the two-layer Gnanadesikan model,

$$t_{\text{adjust}} \sim \left(\frac{\kappa_{\text{GM}} L_x}{A L_y} + \frac{1}{A} \frac{dq_N}{dh} \right)^{-1}, \qquad (16)$$

where h is the depth of the pycnocline in Gnanadesikan's model.

To test the sensitivity of the overall adjustment time scale to the parameterization of NADW formation, we now consider a case in which the rate of NADW formation scales with the square of the pycnocline depth, here taken as the depth of the $\Theta = 6.435°C$ surface. Since the stratification deepens in the warming calculation, NADW formation also increases slightly as the Conservative Temperature surface deepens (Fig. 8b). The peak heat uptake, shown in Fig. 8c, is almost insensitive to the dependence of the NADW on the stratification, but the adjustment time scale decreases, as expected from Eq. (16). In reality, we expect NADW formation to decrease under warming scenarios due to the dependence of the MOC on the meridional density gradient (see de Boer et al. 2010a; Fürst and Levermann 2012), and it is therefore unclear how NADW formation will affect the overall adjustment time scale.

In the two-box model of Held et al. (2010), also used by Geoffroy et al. (2013a,b), the rate of ocean heat uptake is given by the rate of heat exchange between the upper mixed-layer box and deep ocean box. The above analysis provides a dynamical rationale for setting the time scale of this heat exchange, and hence the time scale of the slow component of surface response to forcing, in terms of the Southern Ocean eddy transport and the sensitivity of NADW formation to changes in stratification.

d. Changes in Southern Ocean transports

Both observations (Thompson et al. 2000; Marshall 2003) and coupled ocean–atmosphere models (Kushner et al. 2001) suggest that Southern Ocean winds are strengthening (and shifting poleward) in response to anthropogenic forcing, with consequent impacts on Southern
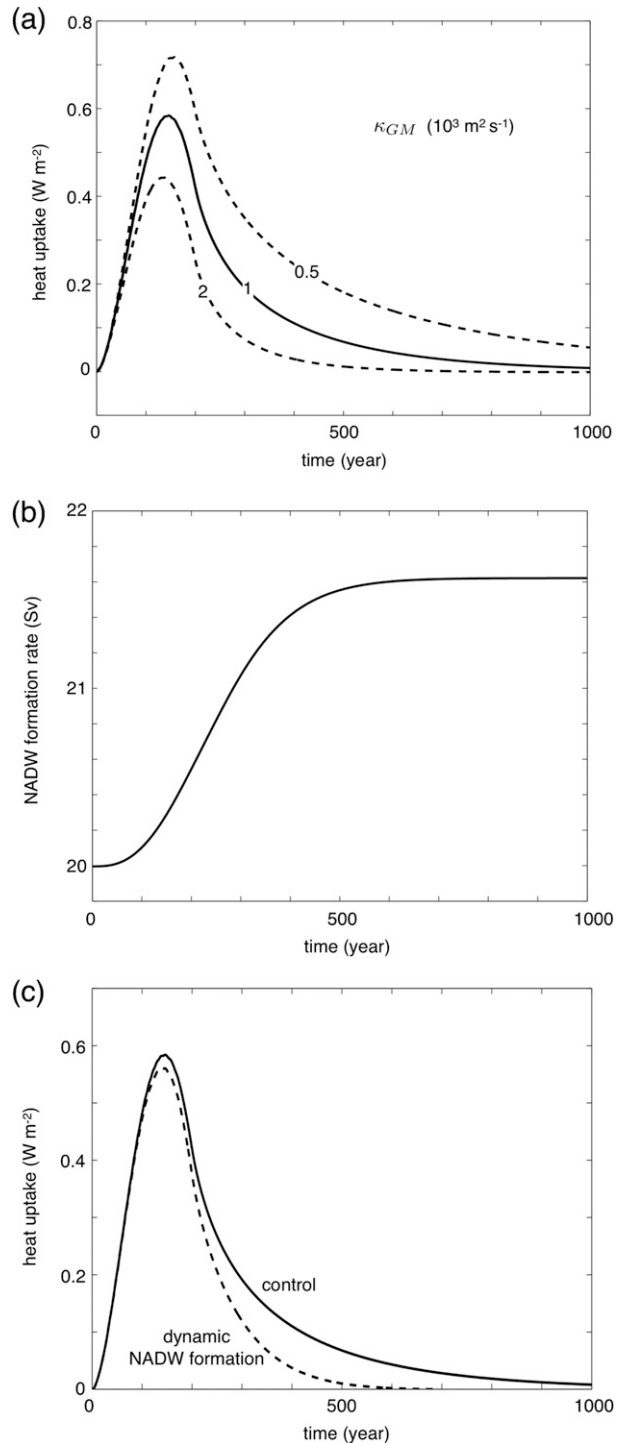

FIG. 8. (a) Ocean heat uptake, normalized by the surface area of Earth, for three different values of the Southern Ocean eddy diffusivity κ_{GM} under the control 4°C warming scenario. (b) Variation of NADW formation (Atlantic MOC strength) with time in a calculation with a dynamic parameterization of the NADW formation rate. (c) Heat uptake of under the prescribed and prognostic NADW parameterizations.

Ocean heat uptake (Fyfe et al. 2007). In Fig. 9b we plot the ocean heat uptake anomaly in an additional scenario in which the Southern Ocean wind stress, and hence the Ekman transport, is increased by 10%. Even though the increase in wind stress is relatively modest, the peak ocean heat uptake increases by almost 50%, and the long-term heat uptake by 100%. Because of the increase in Southern Ocean Ekman transport, the stratification deepens as shown in Fig. 9a, leading to an increase of heat uptake at all depths (Fig. 9c), although the main warming remains in the upper 1.5 km. Unlike in the surface warming-only scenario, the Ekman-induced heat uptake now dominates at most depths with only modest changes from other contributions except for the diapycnal diffusivity contribution in the deep ocean, which is now reduced.

On the other hand, recent results from eddy-permitting ocean models suggest that the Southern Ocean may be in an "eddy saturated" regime in which any increase in Southern Ocean Ekman overturning is compensated by an increase in eddy activity and eddy-induced over-turning, such that the net residual overturning circulation anomaly, $q_{Ek} - q_{Eddy}$, is greatly reduced (e.g., Straub 1993; Hallberg and Gnanadesikan 2006; Farneti et al. 2010; Munday et al. 2013). To address this possibility, in Fig. 9c we also plot the ocean heat uptake anomaly in a scenario in which both the Southern Ocean wind stress and eddy diffusivity increase by 10%. As the increase in eddy diffusivity shallows the stratification, we find that there is a small residual heat uptake, because the Ekman and eddy-induced overturning cells are not exactly com-pensated (especially on shorter time scales), but never-theless the residual heat uptake anomaly is greatly reduced. The impact of the eddy diffusivity on the strat-ification and heat uptake in the CMIP3 ensemble under different forcing scenarios is discussed in Kuhlbrodt and Gregory (2012): their results show that models with small κ_{GM} have a weakened stratification in the Southern Ocean and larger heat uptake efficiency.

e. Changes in NADW formation

One of the greatest uncertainties in the response of the ocean to anthropogenic climate change concerns the response of the Atlantic MOC. Most GCM projections show a warming at high latitudes combined with an in-crease in precipitation leading to an increase in ocean stratification, a reduction in NADW formation and a weakening of the Atlantic MOC (e.g., Gregory et al. 2005). State-of-the-art coupled models show a wide range of plausible behavior, from little change to more than 50% reduction in the Atlantic MOC (Meehl et al. 2007). Thus, in Fig. 10a we show the effect of reducing the rate of NADW formation by 50% and 100%
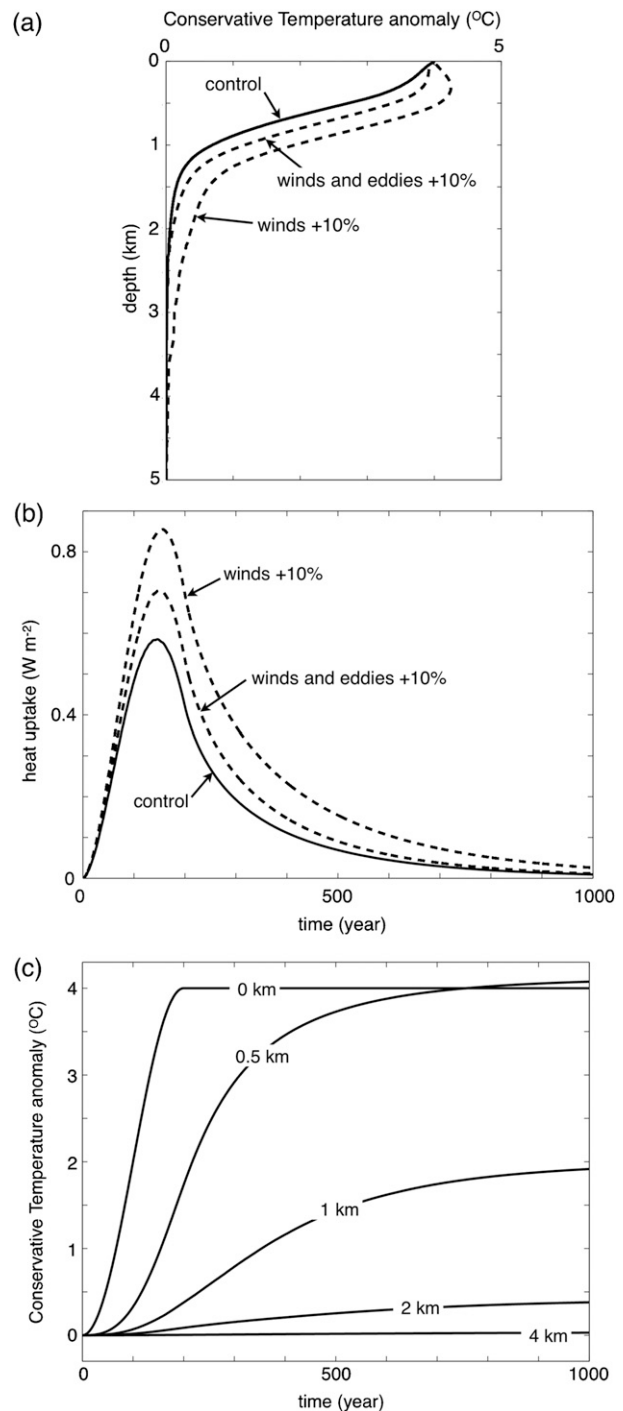

FIG. 9. Calculations quantifying the effects of Southern Ocean winds strengthening by 10% during an anthropogenic forcing sce-nario. Also shown are the effects of simultaneously increasing the eddy diffusivity by 10% following the findings of recent studies in which "eddy compensation" occurs. (a) The initial and final stratification profiles in the three scenarios including the control case with constant Southern Ocean winds and eddies—note that the final profiles are close to, but not in, thermodynamic equilib-rium. (b) Heat uptake, normalized by the surface area of the Earth, in each of the three scenarios. (c) Conservative Temperature anomaly for different layers as function of time under warming scenarios and 10% increase in wind forcing.
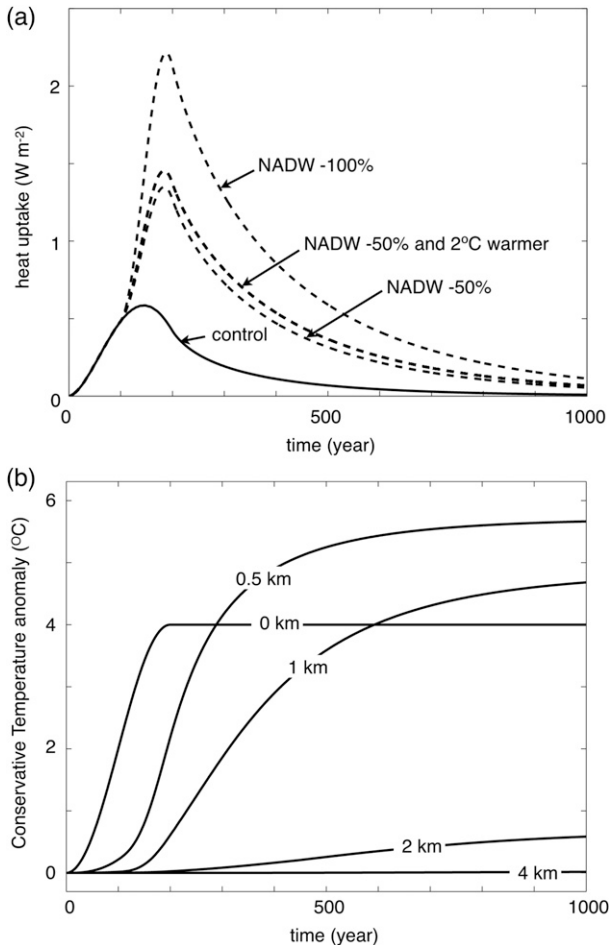
FIG. 10. (a) Heat uptake in three simulations in which NADW formation remains constant at 20 Sv (the control integration), reduces by 50%, and reduces by 100%. (b) Conservative Temperature anomaly for different layers as function of time under warming scenarios and 50% Atlantic MOC reduction.

between years 100 and 200 (over the first 100 years, both of these scenarios are identical to the control). Even a 50% reduction in NADW formation leads to more than a doubling in the peak ocean heat uptake, with an even greater increase with the complete halt of NADW formation.

Figure 10b shows the warming at different depths under a 50% reduction in the NADW formation rate. The striking subsurface warming over the upper 1.5 km is a result of the almost linear stratification in this depth range (Fig. 4c). The deepened stratification increases the heat uptake leading a substantial subsurface warming consistent with Xie and Vallis (2012) and Gregory (2000). The strength of the subsurface heat uptake is associated with the strength and the depth of the Atlantic MOC cell. (Kostov et al. 2014) show using a simple box model and the output of CMIP5 that the upper cell

of the Atlantic MOC is central to transporting and redistributing thermal energy to depth. In their study, the large discrepancies in the strength and depth of the Atlantic MOC in CMIP5 models accounts for the variability in the vertical distribution of ocean heat storage.

We additionally show a scenario in which NADW is formed at a reduced rate (by 50%) and into a warmer Conservative Temperature class (4°–8°C vs 2°–6°C). The effect of warmer NADW appears to be secondary, consistent with the findings in section 3 for the equilibrium solutions (Fig. 4e).

f. Impact of large diapycnal diffusion

Finally, although observations point toward diapycnal mixing rates on the order of $10^{-5} \, m^2 \, s^{-1}$ over the upper ocean, with higher values in the abyss, here we consider the effect of increasing the diapycnal diffusivity to $10^{-4} \, m^2 \, s^{-1}$. This is for two reasons: 1) truncation errors in advection schemes lead to spurious implicit diapycnal mixing (Griffies et al. 2000), even when run at eddy-permitting resolutions [Roberts and Marshall 1998; see Ilicak et al. (2012) for a recent update, including analysis of spurious mixing in global ocean climate simulations], and 2) artificially large "effective diffusivities" are often applied in simple climate models as a parameterization of advective processes.

In Fig. 11 we show the vertical Conservative Temperature profiles from climatological observations and the model with a uniform diapycnal diffusivity of $\kappa_v = 1 \times 10^{-4} \, m^2 \, s^{-1}$, both with and without Southern Ocean winds and eddies. We see that the ocean becomes unrealistically warm in both cases. In Figs. 11b and 11c we show the net heat uptake and its decomposition for the cases with and without Southern Ocean winds and eddies respectively. Consistent with Nikurashin and Vallis (2011, 2012), we find that for large mixing, the contribution of diapycnal mixing becomes comparable to that of the Southern Ocean winds (Ekman transport) in setting the stratification. In Fig. 11c, we see that one can qualitatively model the effect of the Southern Ocean Ekman and eddy-induced overturning cells on heat uptake in our simple 1D model through enhanced effective diffusivity over the upper ocean. This is simply a reflection of the low-order nature of the transient response of our model integration and the ability of any low-order model to fit a smooth curve given sufficient tunable parameters. The peak ocean heat uptake is comparable to the value from the control solution with imposed surface forcing (cf. Fig. 6c).

5. Application to an Earth system model

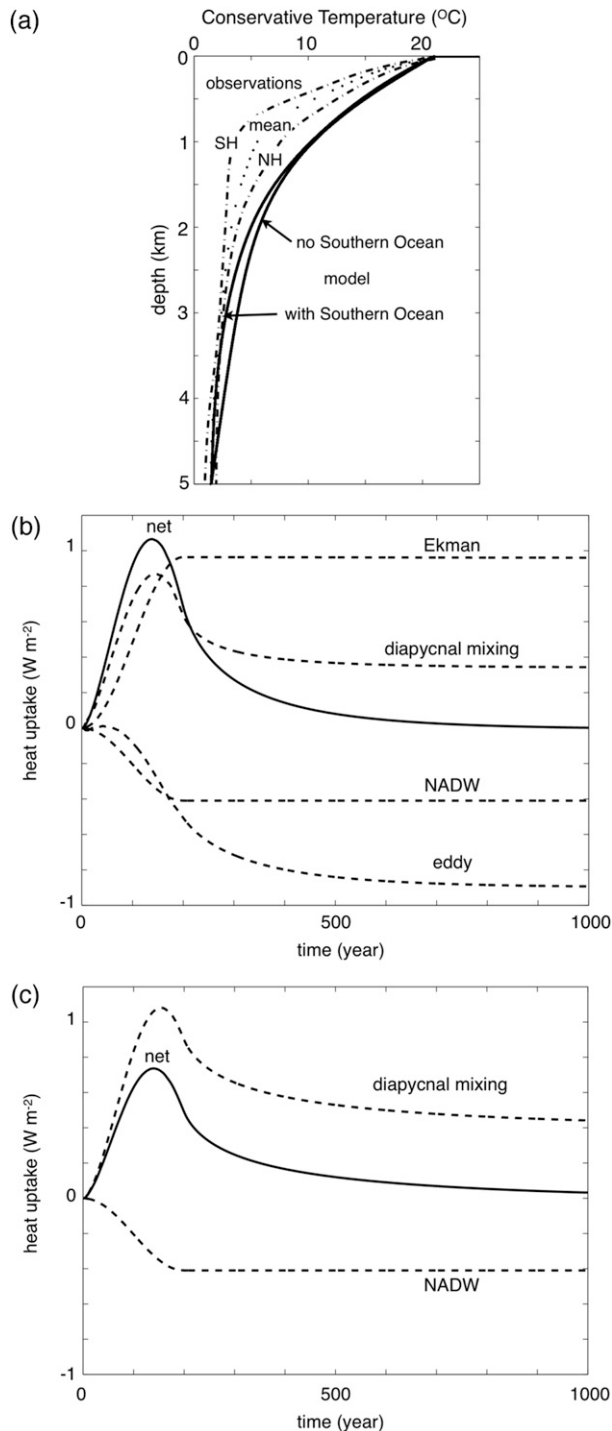To illustrate the utility of the conceptual model to analyze ocean heat uptake in more complex models, we

FIG. 11. Results of two anthropogenic forcing calculations with uniform high diapycnal mixing, $\kappa_v = 1 \times 10^{-4}\,\mathrm{m}^2\,\mathrm{s}^{-1}$, with Southern Ocean winds and eddies turned on and off. (a) Conservative Temperature profiles as a function of depth for the two model calculations, together with the observed climatological profiles in the Atlantic as in Fig. 3 (b) Net ocean heat uptake, normalized by the surface area of Earth, and its decomposition into constituent processes, with Southern Ocean winds and eddies turned on. (c) Net ocean heat uptake and its decomposition in the case with Southern Ocean winds and eddies turned off.

now apply it to the output of a climate model, the Second Generation Canadian Earth System Model (CanESM2), which has been employed in the Intergovernmental Panel on Climate Change (IPCC) Fifth Assessment Report (Stocker et al. 2013) and is composed of ocean, sea ice, atmosphere, land, and carbon cycle components. The ocean component of CanESM2 is the National Center for Atmospheric Research (NCAR) Community Ocean Model (Gent et al. 1998), based on the Geophysical Fluid Dynamics Laboratory Modular Ocean Model. The resolution of the model is 1.418° (longitude) × 0.948° (latitude) with 40 vertical levels of varying thicknesses from 10 m near the surface to roughly 400 m in the abyss. Eddies are parameterized using Gent and McWilliams (1990) with a spatially uniform eddy diffusivity, $\kappa_{GM} = 10^3\,\mathrm{m}^2\,\mathrm{s}^{-1}$. Diapycnal mixing driven by buoyancy and shear is parameterized by the K-profile parameterization (KPP) scheme (Large et al. 1994) in the surface mixed layer (ignored in our 1D model) and the Simmons et al. (2004) parameterization of diapycnal mixing.

The control integration of CanESM2 is used to fit the 1D model. Southern Ocean Ekman transport and NADW formation rates are estimated from the control integration averaged over the last 100 years, defined through the maximum Eulerian meridional overturning strengths between 45° and 60°S and between 45° and 60°N respectively. The diapycnal diffusivity profile in the GCM is calculated dynamically using Simmons et al.'s (2004) calculation and varies with latitude, longitude, and time; instead, we mimic the mean effect of the parameterization by crudely modeling the diapycnal diffusivity profile in Fig. 1 of Simmons et al. (2004). To do so, we prescribe a uniform value of $3 \times 10^{-5}\,\mathrm{m}^2\,\mathrm{s}^{-1}$ over the upper 3 km, increasing linearly to $7.7 \times 10^{-4}\,\mathrm{m}^2\,\mathrm{s}^{-1}$ between 3 and 5 km. All of the remaining parameters have the same values as used in the control integration in sections 3 and 4, except that the bottom Conservative Temperature is set to 0° here, consistent with the vertical potential temperature profile from the GCM.

In Fig. 12a, we show the initial stratification of the 1D model along with those from the GCM in the North and South Atlantic at the start of the transient experiment. These curves are chosen for consistency with Fig. 3, but also because the heat uptake is dominated by the Atlantic sector in both hemispheres in the GCM (not shown). The stratification in the 1D model is too deep between 0.5 and 1.5 km, and likewise beneath 3 km, which we have been unable to reconcile but most likely results from ambiguities in defining the overall magnitudes of the Southern Ocean Ekman transport and NADW formation.

The 1D model is then forced with the time series of sea surface temperature, Southern Ocean Ekman transport,
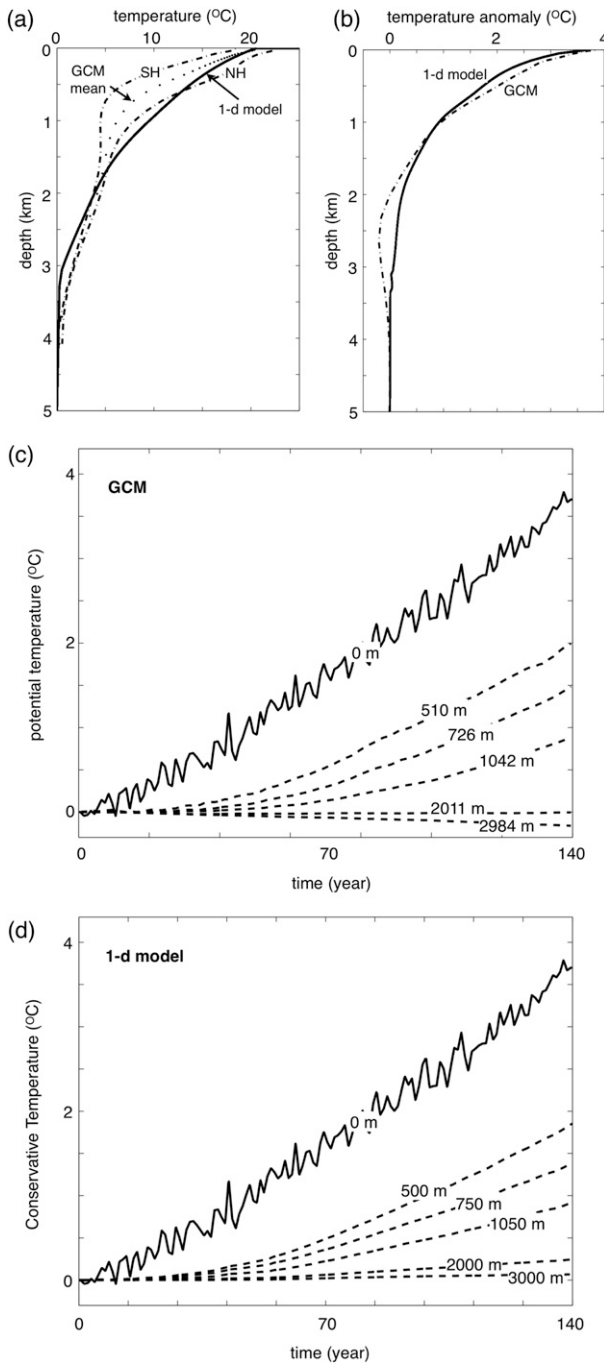
FIG. 12. (a) Initial Conservative Temperature profile from the 1D model when fitted with the GCM control fields (solid line). For comparison, the initial potential temperature profiles diagnosed from the GCM are shown between 20° and 40° in the Atlantic (dashed lines) in each hemisphere, along with their mean (dotted line). (b) Conservative Temperature anomaly over the 140-yr integration in the 1D model (solid line) and mean potential temperature anomaly between 40°S and 60°N in the GCM (dashed line). (c) Potential temperature anomalies as a function of time at various depths in the GCM, averaged between 40°S and 60°N. (d) Conservative Temperature anomalies as a function of time at similar depths in the 1D model.

and NADW formation diagnosed from a GCM simulation in which the atmospheric CO_2 concentration is increased by 1% yr^{-1}, starting from the preindustrial control state until the CO_2 concentration reaches 4 times its preindustrial value. The length of the time series is 140 years. The bolus eddy transport is calculated dynamically in the 1D model with a constant diffusivity, $\kappa_{GM} = 1 \times 10^3 \, \text{m}^2 \, \text{s}^{-1}$ as used in the CanESM2.

Despite the discrepancies between the initial stratification profiles in the 1D model and GCM, the vertical temperature profile of the warming over the 140 years of integration, agrees remarkably well between the 1D model and GCM (Fig. 12b), except that the GCM warms slightly more over the upper 1 km and actually cools at depth below 2 km. The latter is partly due to a change in the strength of the AABW cell in the GCM (not shown) which the 1D model is incapable of capturing at present. In Figs. 12c and 12d, we see that the temporal variation of the warming also compares favorably between the GCM and 1D model at different depths with errors of less than 0.1°C (except in abyssal layers, where the sign of the temperature change is incorrect as described above).

The simple 1D model provides yet a reliable first-order approximation of the model heat uptake in a transient climate change experiment. Figures 13a and 13b show the ocean heat uptake time series from the GCM averaged globally and over 40°S–60°N (where the 1D model is valid), respectively. Most of the heat uptake, roughly 1.6 W m^{-2} at the end of the forced integration over latitudes 40°S–60°N, is concentrated in the upper 2 km (0.9 W m^{-2} between 0 and 0.7 km and 0.6 W m^{-2} between 0.7 and 2 km) and with negligible uptake at depth. The results from the 1D model shown in Fig. 13c for the heat uptake compare extremely well with the GCM output as expected from the temperature time series (Figs. 12c,d).

Various simple metrics are used to evaluate the response of models to forcing, especially when comparing GCMs output with simple models. The "ocean heat uptake efficiency" quantifies the rate at which heat is transported downward and provides a good measure of a model's response to slowly varying radiative forcing. The heat uptake efficiency calculated in CanESM2 is about 0.56 W m^{-2} K^{-1} (Kuhlbrodt and Gregory 2012; Forster et al. 2013). The 1D model heat efficiency is 0.47 W m^{-2} K^{-1}, slightly below the estimated value due to the exclusion of the Southern Ocean and northern high-latitude basins. The GCM output shows an increase in the Southern Ocean Ekman transport and as expected, Ekman pumping entirely dominates the ocean heat uptake, shown in Fig. 13d. The sink of heat due to Southern Ocean eddies increases (due to the decrease in
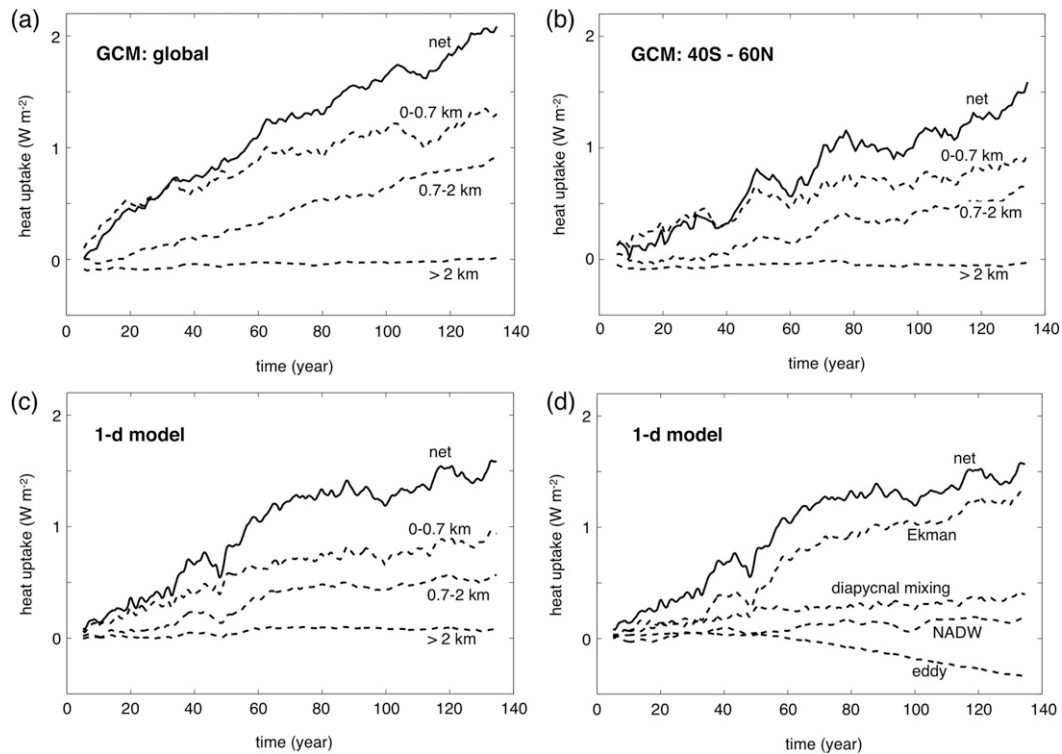
FIG. 13. (a) Net global ocean heat uptake, normalized by the surface area of Earth in the GCM, and decomposed into layers between 0 and 0.7, 0.7 and 2, and 2 and 5 km. (b) As in (a), but between 40°S and 60°N in order to exclude the Southern Ocean and high-latitude northern basins where the 1D model is not applicable. (c) Net ocean heat uptake in the 1D model and decomposed over the same layers. (d) Net ocean heat uptake in the 1D model due to Southern Ocean Ekman transport, NADW formation, Southern Ocean eddies, and diapycnal mixing.

the eddy bolus transport) but is nearly balanced by the contributions from NADW (i.e., weakening of the Atlantic MOC) and diapycnal mixing.

To further understand the role of NADW and Ekman pumping as sources of ocean heat uptake, the 1D model is initialized solely with the GCM NADW time series, excluding the Southern Ocean processes. The initial stratification of the 1D model agrees extremely well with GCM stratification profiles in the Atlantic (Fig. 14a). However, the final stratification profile of the 1D model disagrees with the GCM, especially between 0.7 and 2 km (Fig. 14b), resulting in an underestimate of net ocean heat uptake by about 50% (Fig. 14c). This experiment highlights the importance of the Southern Ocean Ekman water mass transformation in determining the transient ocean heat uptake and its vertical distribution.

When Southern Ocean processes are turned off, the model is now equivalent to an upwelling-diffusion model with uniform enhanced mixing $\kappa_v = 1 \times 10^{-4} \, \mathrm{m^2 \, s^{-1}}$. The initial and final ocean stratifications obtained in this configuration of the 1D model are farther away from that of the GCM (Figs. 15a,b). However the net ocean heat uptake, reaching $1.4 \, \mathrm{W \, m^{-2}}$ at the end of the experiment,

matches fairly well the ocean heat uptake from the simple model with the Southern Ocean processes and weaker mixing (cf. Figs. 15c and 13c). The heat uptake over the upper 0.7 km is in broad agreement with the GCM results owing to the almost linear stratification over the upper ocean; however, the heat uptake between 0.7 and 2 km is underestimated by more than 30%.

6. Discussion

In this paper, we have developed a conceptual model as a multilayer generalization of Gnanadesikan (1999) to analyze the dynamical processes controlling ocean heat uptake under various climate change scenarios. The model represents the role of the Southern Ocean Ekman and eddy transports, the Atlantic MOC, and diapycnal mixing in setting the ocean stratification and consequently the rate of ocean heat uptake.

For realistic profiles of diapycnal mixing, the ocean heat uptake remains mostly confined to the upper 2 km of the ocean for several centuries and is dominated by the wind-induced Ekman transport in the Southern Ocean; its adjustment time scale is set mostly by the
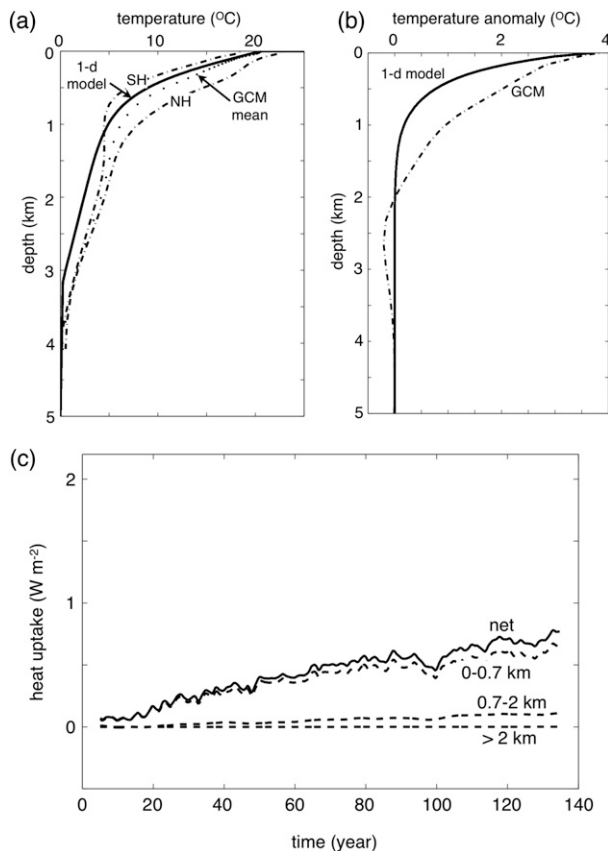
FIG. 14. (a) Initial Conservative Temperature profile in the 1D model when initialized with the GCM NADW time series, but excluding Southern Ocean processes, along with Atlantic potential temperature profiles as in Fig. 12a. Diapycnal mixing is enhanced at depth as in the control experiment. (b) Conservative Temperature anomaly over the 140-yr integration in the 1D model (solid line) and mean potential temperature anomaly between 40°S and 60°N in the GCM (dashed line). (c) Net ocean heat uptake, normalized by the surface area of Earth, along with the heat uptake between 0 and 0.7, 0.7 and 2, and 2 and 5 km.
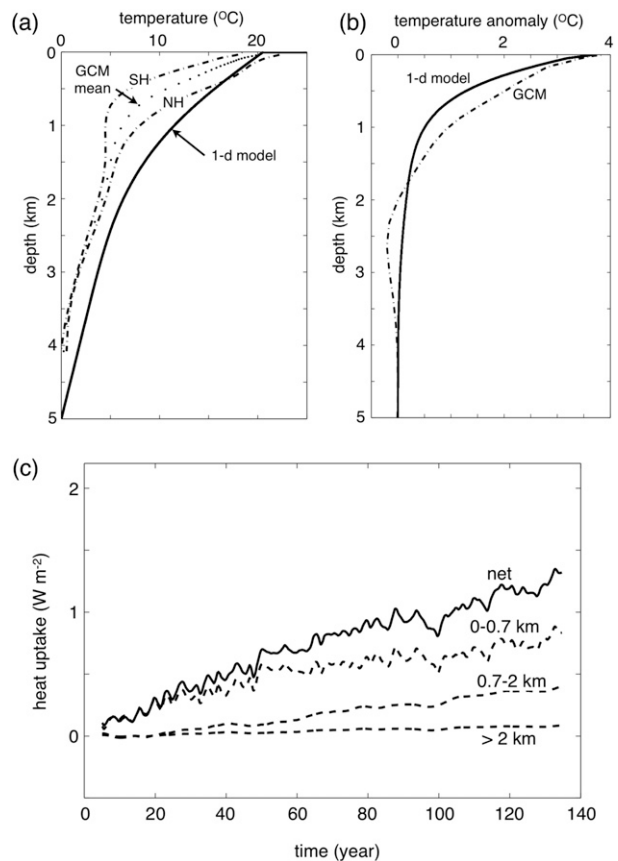
FIG. 15. (a) Initial and (b) final stratification of the simple model when initialized with the GCM output without any Southern Ocean processes and uniform enhanced mixing, $\kappa_v = 1 \times 10^{-4}\,\mathrm{m^2\,s^{-1}}$. For comparison, the initial and final profiles of Atlantic and Pacific stratification directly from the GCM are also shown. (c) Net ocean heat uptake, normalized by the surface area of Earth, along with the ocean heat uptake between 0 and 0.7, 0.7 and 2, and 2 and 5 km.

Southern Ocean eddy transport and the sensitivity of NADW formation to changes in stratification. The model suggests that any future increase in wind stress over the Southern Ocean under climate change will likely increase ocean heat uptake by deepening the stratification. However, the rate of uptake will be greatly reduced due to the compensating effect of the Southern ocean eddy bolus transport. A recent study by Balmaseda et al. (2013) analyzed the impact of removing interannual variability of the wind over the global ocean on a re-analysis product of ocean heat content between 1990 and 2009, obtaining a reduction of the overall heat uptake of up 60%, as well as reduced penetration of heat below 300 m in low latitudes. This result further emphasizes the impact of the surface wind stress on the global ocean heat uptake and the vertical profile of the warming.

If the diapycnal diffusivity is artificially enhanced in the model, as is sometimes the case in simple models, or in GCMs due to numerical truncation errors (Ilicak et al. 2012), the contribution of diapycnal mixing to net ocean heat uptake becomes comparable to, if not larger than, that of the Southern Ocean Ekman transport. Gregory (2000) investigated changes in ocean heat uptake on de-cadal time scales in the Hadley Centre Coupled Model, version 2 (HadCM2), showing that the wind-driven circulation in the Southern Ocean dominated the vertical exchange of heat in the control experiment. However, the anomalous heat uptake under a 1% CO_2 increase within the same model was dictated by changes in high-latitude convection leading to subsurface warming and net heat uptake; the secondary role of the Ekman transport in this experiment is perhaps due to the enhanced diffusive processes and the lack of a parameterization of the eddy bolus velocity.

The potential reduction in the rate of NADW formation and, therefore, weakening of the MOC in the North Atlantic, has been shown to deepen the stratification, substantially increasing the subsurface warming and the overall heat uptake, similar to the impact of increasing the Southern Ocean wind stress. Various studies have pointed out the influence of high-latitude convection in the North Atlantic and the reduction of the MOC on the regional and global heat uptake (e.g., Manabe et al. 1991; Knutti and Tomassini 2008; Xie and Vallis 2012).

We have further shown that high values of diapycnal diffusivity in low-order models can mimic the effect of the Southern Ocean Ekman transport on the integrated ocean heat uptake such that the contributions of diapycnal mixing and Southern Ocean Ekman transport to the net heat uptake are comparable, but the stratification extends unrealistically to the sea floor.

The results are confirmed when the output of a GCM is analyzed using the 1D conceptual model. The 1D model is forced by time series of sea surface temperature, Southern Ocean Ekman transport, and NADW formation, diagnosed from an integration of CanESM2 in which atmospheric CO_2 is increased by $1\% \, \mathrm{yr}^{-1}$ to 4 times its preindustrial value. The Southern Ocean Ekman transport is found to be essential to reproduce in the 1D model the magnitude and vertical profile of ocean heat uptake obtained in the GCM.

In summary, our study suggests that changes of high-latitude dynamical processes have a strong influence on the global stratification and the ocean heat uptake and its vertical distribution. In contrast, the contribution of diapycnal mixing in maintaining the ocean stratification and the ocean heat uptake is of secondary importance.

We have not addressed the impact of variability in surface wind stress and MOC changes due to NADW formation on ocean heat uptake and, in particular, whether this can explain the slowing down of surface warming observed over the past decade (e.g., Meehl et al. 2007). Moreover, the conceptual model can only be used as a diagnostic tool to analyze the ocean heat content and presently cannot include feedbacks between the ocean and atmospheric radiative forcing because the surface temperature variation is prescribed. We plan to modify the model in a future study to include such feedbacks in order to explore how the rate of surface warming varies under different anthropogenic forcing scenarios.

A further potential application of the model is climate change over different geological periods such as a the Last Glacial Maximum in which changes in the strength of AABW are believed to have played an important role (e.g., Toggweiler et al. 2006; de Boer et al. 2010b; Ferrari et al. 2014). While the model does not yet have an explicit parameterization of AABW formation, the latter might be prescribed in a similar manner to the prescription of NADW formation rates in the present paper, although there are issues surrounding how such a prescription might interact with the parameterization of Southern Ocean eddy transports. Moreover, such a model might be extended to incorporate biogeochemical tracers following the approach of Goodwin (2012).

Finally, we hope that the conceptual 1D model developed in this manuscript, in which ocean circulation and associated water mass transformation are fundamental to reproducing the vertical structure and time scale of adjustment of ocean heat uptake, might replace the "upwelling diffusion" slab models and simple box models in which nondiffusive vertical heat transports are represented through enhanced vertical diffusion.

REFERENCES

Allison, L., H. Johnson, D. Marshall, and D. Munday, 2010: Where do winds drive the Antarctic Circumpolar Current? *Geophys. Res. Lett.,* **37,** L12605, doi:10.1029/2010GL043355.

——, ——, and ——, 2011: Spin-up and adjustment of the Antarctic Circumpolar Current and global pycnocline. *J. Mar. Res.,* **69,** 167–189, doi:10.1357/002224011798765330.

Balmaseda, M. A., K. E. Trenberth, and E. Källén, 2013: Distinctive climate signals in reanalysis of global ocean heat content. *Geophys. Res. Lett.,* **40,** 1754–1759, doi:10.1002/grl.50382.

Banks, H. T., and J. M. Gregory, 2006: Mechanisms of ocean heat uptake in a coupled climate model and the implications for tracer based predictions of ocean heat uptake. *Geophys. Res. Lett.,* **33,** L07608, doi:10.1029/2005GL025352.

Boé, J., A. Hall, and X. Qu, 2009: Deep ocean heat uptake as a major source of spread in transient climate change simulations. *Geophys. Res. Lett.,* **36,** L22701, doi:10.1029/2009GL040845.

Bryan, K., and L. J. Lewis, 1979: A water mass model of the world ocean. *J. Geophys. Res.,* **84,** 2503–2517, doi:10.1029/JC084iC05p02503.

Charney, J. G., and Coauthors, 1979: Carbon dioxide and climate: A scientific assessment. Report of an ad hoc study on carbon dioxide and climate, for the Climate Research Board, National Research Council, 22 pp.

Church, J. A., J. S. Godfrey, D. R. Jackett, and T. J. McDougall, 1991: A model of sea-level rise caused by ocean thermal expansion. *J. Climate,* **4,** 438–456, doi:10.1175/1520-0442(1991)004<0438:AMOSLR>2.0.CO;2.

Dalan, F., P. H. Stone, and A. P. Sokolov, 2005: Sensitivity of the ocean's climate to diapycnal diffusivity in an EMIC. Part II:

Global warming scenario. *J. Climate,* **18,** 2482–2496, doi:10.1175/JCLI3412.1.

Danabasoglu, G., J. C. McWilliams, and P. R. Gent, 1994: The role of mesoscale tracer transport in the global ocean circulation. *Science,* **264,** 1123–1126, doi:10.1126/science.264.5162.1123.

de Boer, A., A. Gnanadesikan, N. Edwards, and A. Watson, 2010a: Meridional density gradients do not control the Atlantic overturning circulation. *J. Phys. Oceanogr.,* **40,** 368–380, doi:10.1175/2009JPO4200.1.

——, A. J. Watson, N. R. Edwards, and K. I. C. Oliver, 2010b: A multivariable box model approach to the soft tissue carbon pump. *Climate Past,* **6,** 827–841, doi:10.5194/cp-6-827-2010.

Durran, D. R., 1991: The third-order Adams–Bashforth method: An attractive alternative to leapfrog time differencing. *Mon. Wea. Rev.,* **119,** 702–720, doi:10.1175/1520-0493(1991)119<0702:TTOABM>2.0.CO;2.

Farneti, R., T. L. Delworth, A. Rosati, S. M. Griffies, and F. Zeng, 2010: The role of mesoscale eddies in the rectification of the Southern Ocean response to climate change. *J. Phys. Oceanogr.,* **40,** 1539–1557, doi:10.1175/2010JPO4353.1.

Ferraria, R., M. F. Jansen, J. F. Adkins, A. Burke, A. L. Stewart, and A. F. Thompson, 2014: Antarctic sea ice control on ocean circulation in present and glacial climates. *Proc. Natl. Acad. Sci. USA,* **111,** 8753–8758, doi:10.1073/pnas.1323922111.

Forster, P. M., T. Andrews, P. Good, J. M. Gregory, L. S. Jackson, and M. Zelinka, 2013: Evaluating adjusted forcing and model spread for historical and future scenarios in the CMIP5 generation of climate models. *J. Geophys. Res. Atmos.,* **118,** 1139–1150, doi:10.1002/jgrd.50174.

Fürst, J. J., and A. Levermann, 2012: A minimal model for wind- and mixing-driven overturning: Threshold behavior for both driving mechanisms. *Climate Dyn.,* **38,** 239–260, doi:10.1007/s00382-011-1003-7.

Fyfe, J. C., O. A. Saenko, K. Zickfeld, M. Eby, and A. J. Weaver, 2007: The role of poleward-intensifying winds on Southern Ocean warming. *J. Climate,* **20,** 5391–5400, doi:10.1175/2007JCLI1764.1.

Gent, P., and J. C. McWilliams, 1990: Isopycnal mixing in ocean circulation models. *J. Phys. Oceanogr.,* **20,** 150–155, doi:10.1175/1520-0485(1990)020<0150:IMIOCM>2.0.CO;2.

——, F. Bryan, G. Danabasoglu, S. Doney, W. Holland, W. Large, and J. McWilliams, 1998: The NCAR Climate System Model global ocean component. *J. Climate,* **11,** 1287–1306, doi:10.1175/1520-0442(1998)011<1287:TNCSMG>2.0.CO;2.

Geoffroy, O., D. Saint-Martin, D. J. L. Olivié, A. Voldoire, G. Bellon, and S. Tytéca, 2013a: Transient climate response in a two-layer energy-balance model. Part I: Analytical solution and parameter calibration using CMIP5 AOGCM experiments. *J. Climate,* **26,** 1841–1857, doi:10.1175/JCLI-D-12-00195.1.

——, ——, ——, ——, ——, and ——, 2013b: Transient climate response in a two-layer energy-balance model. Part II: Representation of the efficacy of deep-ocean heat uptake and validation for CMIP5 AOGCMs. *J. Climate,* **26,** 1859–1876, doi:10.1175/JCLI-D-12-00196.1.

Gnanadesikan, A., 1999: A simple predictive model of the structure of the oceanic pycnocline. *Science,* **283,** 2077–2081, doi:10.1126/science.283.5410.2077.

——, R. D. Slater, P. S. Swathi, and G. K. Vallis, 2005: The ocean circulation in thermohaline coordinates. *J. Climate,* **18,** 2604–2616, doi:10.1175/JCLI3436.1.

Goodwin, P., 2012: An isopycnal box model with predictive deep-ocean structure for biogeochemical cycling applications. *Ocean Modell.,* **51,** 19–36, doi:10.1016/j.ocemod.2012.04.005.

Gouretski, V. V., and K. P. Kolterman, 2004: WOCE global hydrographic climatology. Berichte des Bundesamtes Seeschifffahrt und Hydrographie Rep. 35. [Available online at http://odv.awi.de/en/data/ocean/woce_global_hydrographic_climatology/.]

Graham, F. S., and T. J. McDougall, 2013: Quantifying the non-conservative production of Conservative Temperature, potential temperature, and entropy. *J. Phys. Oceanogr.,* **43,** 838–862, doi:10.1175/JPO-D-11-0188.1.

Gregory, J. M., 2000: Vertical heat transports in the ocean and their effect on time-dependent climate change. *Climate Dyn.,* **16,** 501–515, doi:10.1007/s003820000059.

——, and Coauthors, 2005: A model intercomparison of changes in the Atlantic thermohaline circulation in response to increasing atmospheric CO_2 concentration. *Geophys. Res. Lett.,* **32,** L23605, doi:10.1029/2005GL023209.

Griffies, S. M., R. C. Paconowski, and R. W. Hallberg, 2000: Spurious diapycnal mixing associated with advection in a z-coordinate ocean model. *Mon. Wea. Rev.,* **128,** 538–564, doi:10.1175/1520-0493(2000)128<0538:SDMAWA>2.0.CO;2.

Hallberg, R., and A. Gnanadesikan, 2006: The role of eddies in determining the structure and response of the wind-driven Southern Hemisphere overturning: Results from the Modeling Eddies in the Southern Ocean (MESO) project. *J. Phys. Oceanogr.,* **36,** 2232–2252, doi:10.1175/JPO2980.1.

Hansen, J., G. Russell, A. Lacis, I. Fung, and D. Rind, 1985: Climate response times: Dependence on climate sensitivity and ocean mixing. *Science,* **229,** 857–859, doi:10.1126/science.229.4716.857.

Harvey, L. D. D., and S. H. Schneider, 1985: Transient climate response to external forcing on 10^0 to 10^4 year time scales. Part 1: Experiments with globally averaged, coupled, atmosphere and ocean energy balance models. *J. Geophys. Res.,* **90,** 2191–2205, doi:10.1029/JD090iD01p02191.

Hasselmann, K., R. Sausen, E. Maier-Reimer, and R. Voss, 1993: On the cold start problem in transient simulations with coupled atmosphere–ocean models. *Climate Dyn.,* **9,** 53–61, doi:10.1007/BF00210008.

Held, I. M., M. Winton, K. Takahashi, T. Delworth, F. Zeng, and G. K. Vallis, 2010: Probing the fast and slow components of global warming by returning abruptly to preindustrial forcing. *J. Climate,* **23,** 2418–2427, doi:10.1175/2009JCLI3466.1.

Hoffert, M. I., A. J. Callegari, and C.-T. Hsieh, 1980: The role of deep sea heat storage in the secular response to climatic forcing. *J. Geophys. Res.,* **85,** 6667–6679, doi:10.1029/JC085iC11p06667.

Huang, B. Y., P. H. Stone, A. P. Sokolov, and I. V. Kamenkovich, 2003: The deep-ocean heat uptake in transient climate change. *J. Climate,* **16,** 1352–1363, doi:10.1175/1520-0442-16.9.1352.

Ilicak, M., A. J. Adcroft, S. M. Griffies, and R. W. Hallberg, 2012: Spurious dianeutral mixing and the role of momentum closure. *Ocean Modell.,* **45-46,** 37–58, doi:10.1016/j.ocemod.2011.10.003.

Ito, T., and J. Marshall, 2008: Control of lower-limb overturning circulation in the Southern Ocean by diapycnal mixing and mesoscale eddy transfer. *J. Phys. Oceanogr.,* **38,** 2832–2845, doi:10.1175/2008JPO3878.1.

Johnson, H. L., and D. P. Marshall, 2002: A theory for the surface Atlantic response to thermohaline variability. *J. Phys. Oceanogr.,* **32,** 1121–1132, doi:10.1175/1520-0485(2002)032<1121:ATFTSA>2.0.CO;2.

——, ——, and D. A. J. Sproson, 2007: Reconciling theories of a mechanically driven meridional overturning circulation with thermohaline forcing and multiple equilibria. *Climate Dyn.,* **29,** 821–836, doi:10.1007/s00382-007-0262-9.

Jones, D. C., T. Ito, and N. Lovenduski, 2011: The transient response of the Southern Ocean pycnocline to changing

atmospheric winds. *Geophys. Res. Lett.,* **38,** L15604, doi:10.1029/2011GL048145.

Kamenkovich, I., and T. Radko, 2011: Role of the Southern Ocean in setting the Atlantic stratification and meridional overturning circulation. *J. Mar. Res.,* **69,** 277–308, doi:10.1357/002224011798765286.

Knutti, R., and L. Tomassini, 2008: Constraints on the transient climate response from observed global temperature and ocean heat uptake. *Geophys. Res. Lett.,* **35,** L09701, doi:10.1029/2007GL032904.

Kostov, Y., K. C. Armour, and J. Marshall, 2014: Impact of the Atlantic meridional overturning circulation on ocean heat storage and transient climate change. *Geophys. Res. Lett.,* **41,** 2108–2116, doi:10.1002/2013GL058998.

Kuhlbrodt, T., and J. M. Gregory, 2012: Ocean heat uptake and its consequences for the magnitude of sea level rise and climate change. *Geophys. Res. Lett.,* **39,** L18608, doi:10.1029/2012GL052952.

Kushner, P. J., I. M. Held, and T. L. Delworth, 2001: Southern Hemisphere atmospheric circulation response to global warming. *J. Climate,* **14,** 2238–2249, doi:10.1175/1520-0442(2001)014<0001:SHACRT>2.0.CO;2.

Large, W. G., J. McWilliams, and S. Doney, 1994: Oceanic vertical mixing: A review and a model with a nonlocal boundary layer parameterization. *Rev. Geophys.,* **32,** 363–403, doi:10.1029/94RG01872.

Ledwell, J. R., A. J. Watson, and C. S. Law, 1998: Mixing of a tracer in the pycnocline. *J. Geophys. Res.,* **103,** 21 499–21 529, doi:10.1029/98JC01738.

Levitus, S., J. I. Antonov, T. P. Boyer, and C. Stephens, 2000: Warming of the world ocean. *Science,* **287,** 2225–2229, doi:10.1126/science.287.5461.2225.

——, ——, and ——, 2005: Warming of the world ocean, 1955–2003. *Geophys. Res. Lett.,* **32,** L02604, doi:10.1029/2004GL021592.

——, ——, and ——, 2012: World ocean heat content and thermosteric sea level change (0–2000 m), 1955–2010. *Geophys. Res. Lett.,* **39,** L10603, doi:10.1029/2012GL051106.

Li, C., J.-S. von Storch, and J. Marotzke, 2013: Deep-ocean heat uptake and equilibrium climate response. *Climate Dyn.,* **40,** 1071–1086, doi:10.1007/s00382-012-1350-z.

Lumpkin, R., and K. Speer, 2007: Global ocean meridional overturning. *J. Phys. Oceanogr.,* **37,** 2550–2562, doi:10.1175/JPO3130.1.

Manabe, S., R. J. Stouffer, M. J. Spelman, and K. Bryan, 1991: Transient responses of a coupled ocean–atmosphere model to gradual changes of atmospheric CO_2. Part I: Annual mean response. *J. Climate,* **4,** 785–818, doi:10.1175/1520-0442(1991)004<0785:TROACO>2.0.CO;2.

Marotzke, J., 1997: Boundary mixing and the dynamics of three-dimensional thermohaline circulations. *J. Phys. Oceanogr.,* **27,** 1713–1728, doi:10.1175/1520-0485(1997)027<1713:BMATDO>2.0.CO;2.

Marshall, D., 1997: Subduction of water masses in an eddying ocean. *J. Mar. Res.,* **55,** 201–222, doi:10.1357/0022240973224373.

——, and H. L. Johnson, 2013: Propagation of meridional circulation anomalies along western and eastern boundaries. *J. Phys. Oceanogr.,* **43,** 2699–2717, doi:10.1175/JPO-D-13-0134.1.

Marshall, G. J., 2003: Trends in the southern annular mode from observations and reanalyses. *J. Climate,* **16,** 4134–4143, doi:10.1175/1520-0442(2003)016<4134:TITSAM>2.0.CO;2.

Marshall, J., and T. Radko, 2003: Residual-mean solutions for the Antarctic Circumpolar Current and its associated overturning circulation. *J. Phys. Oceanogr.,* **33,** 2341–2354, doi:10.1175/1520-0485(2003)033<2341:RSFTAC>2.0.CO;2.

McDougall, T. J., 2003: Potential enthalpy: A conservative oceanic variable for evaluating heat content and heat fluxes. *J. Phys. Oceanogr.,* **33,** 945–963, doi:10.1175/1520-0485(2003)033<0945:PEACOV>2.0.CO;2.

——, and W. K. Dewar, 1998: Vertical mixing and cabbeling in layered models. *J. Phys. Oceanogr.,* **28,** 1458–1480, doi:10.1175/1520-0485(1998)028<1458:VMACIL>2.0.CO;2.

——, and P. M. Barker, 2011: Getting started with TEOS-10 and the Gibbs seawater (GSW) oceanographic toolbox. SCOR/IAPSO WG127, 28 pp. [Available online at http://www.teos-10.org/publications.htm, under "Introductory Articles on TEOS-10."]

Meehl, G. A., and Coauthors, 2007: Global climate projections. *Climate Change 2007: The Physical Science Basis,* S. Solomon et al., Eds., Cambridge University Press, 747–846.

Munday, D., H. Johnson, and D. P. Marshall, 2013: Eddy saturation of equilibrated circumpolar currents. *J. Phys. Oceanogr.,* **43,** 507–532, doi:10.1175/JPO-D-12-095.1.

Munk, W., 1966: Abyssal recipes. *Deep-Sea Res.,* **13,** 707–730.

——, and C. Wunsch, 1998: Abyssal recipes II: Energetics of tidal and wind mixing. *Deep-Sea Res.,* **45,** 1977–2009, doi:10.1016/S0967-0637(98)00070-3.

Naveira Garabato, A. C., K. L. Polzin, B. A. King, K. J. Heywood, and M. Visbeck, 2004: Widespread intense turbulent mixing in the Southern Ocean. *Science,* **303,** 210–213, doi:10.1126/science.1090929.

Nikurashin, M., and G. Vallis, 2011: A theory of deep stratification and overturning circulation in the ocean. *J. Phys. Oceanogr.,* **41,** 485–502, doi:10.1175/2010JPO4529.1.

——, and ——, 2012: A theory of the interhemispheric meridional overturning circulation and associated stratification. *J. Phys. Oceanogr.,* **42,** 1652–1667, doi:10.1175/JPO-D-11-0189.1.

Polzin, K. L., J. M. Toole, J. R. Ledwell, and R. W. Schmidt, 1997: Spatial variability of turbulent mixing in the abyssal ocean. *Science,* **276,** 93–96, doi:10.1126/science.276.5309.93.

Purkey, S. G., and G. C. Johnson, 2010: Warming of global abyssal and deep Southern Ocean waters between the 1990s and 2000s: Contributions to global heat and sea level rise budgets. *J. Climate,* **23,** 6336–6351, doi:10.1175/2010JCLI3682.1.

Radko, T., and I. Kamenkovich, 2011: Semi-adiabatic model of the deep stratification and meridional overturning. *J. Phys. Oceanogr.,* **41,** 757–780, doi:10.1175/2010JPO4538.1.

Raper, S. C. B., and U. Cubasch, 1996: Emulation of the results from a coupled general circulation model using a simple climate model. *Geophys. Res. Lett.,* **23,** 1107–1110, doi:10.1029/96GL01065.

——, J. M. Gregory, and T. J. Osborn, 2001: Use of an upwelling-diffusion energy balance climate model to simulate and diagnose A/OGCM results. *Climate Dyn.,* **17,** 601–613, doi:10.1007/PL00007931.

Roberts, M., and D. Marshall, 1998: Do we require adiabatic dissipation schemes in eddy-resolving ocean models? *J. Phys. Oceanogr.,* **28,** 2050–2063, doi:10.1175/1520-0485(1998)028<2050:DWRADS>2.0.CO;2.

Rogelj, J., M. Meinshausen, and R. Knutti, 2012: Global warming under old and new scenarios using IPCC climate sensitivity range estimates. *Nat. Climate Change,* **2,** 248–253, doi:10.1038/nclimate1385.

Rugenstein, M. A. A., M. Winton, R. J. Stouffer, S. M. Griffies, and R. Hallberg, 2013: Northern high-latitude heat budget decomposition and transient warming. *J. Climate,* **26,** 609–621, doi:10.1175/JCLI-D-11-00695.1.

Samelson, R. M., 2011: Time-dependent adjustment in a simple model of the mid-depth meridional overturning cell. *J. Phys. Oceanogr.,* **41,** 1009–1025, doi:10.1175/2010JPO4562.1.

——, and G. K. Vallis, 1997: Large-scale circulation with small diapycnal diffusion: The two-thermocline limit. *J. Mar. Res.,* **55,** 223–275, doi:10.1357/0022240973224382.

Sandström, J. W., 1916: Meteorologische studien—à schedischen hochgebirge. *Göteborgs K. Vetensk. Vitterhets-Samh. Handl.,* **10,** 2–42.

Shakespeare, C. J., and A. M. Hogg, 2012: An analytical model of the response of the meridional overturning circulation to changes in wind and buoyancy forcing. *J. Phys. Oceanogr.,* **42,** 1270–1287, doi:10.1175/JPO-D-11-0198.1.

Simmons, H. L., S. R. Jayne, L. C. S. Laurent, and A. J. Weaver, 2004: Tidally driven mixing in a numerical model of the ocean general circulation. *Ocean Modell.,* **6,** 245–263, doi:10.1016/S1463-5003(03)00011-8.

Stocker, T. F., and Coauthors, Eds., 2013: *Climate Change 2013: The Physical Science Basis.* Cambridge University Press, 1535 pp.

Straub, D., 1993: On the transport and angular momentum balance of channel models of the Antarctic Circumpolar Current. *J. Phys. Oceanogr.,* **23,** 776–782, doi:10.1175/1520-0485(1993)023<0776:OTTAAM>2.0.CO;2.

Thompson, D. W. J., J. M. Wallace, and G. C. Hegerl, 2000: Annular modes in the extratropical circulation. Part II: Trends. *J. Climate,* **13,** 1018–1036, doi:10.1175/1520-0442(2000)013<1018:AMITEC>2.0.CO;2.

Toggweiler, J. R., J. L. Russell, and S. R. Carson, 2006: Midlatitude westerlies, atmospheric CO_2, and climate change during the ice ages. *Paleoceanography,* **21,** PA2005, doi:10.1029/2005PA001154.

Tziperman, E., 1986: On the role of interior mixing and air–sea fluxes in determining the stratification and circulation of the oceans. *J. Phys. Oceanogr.,* **16,** 680–693, doi:10.1175/1520-0485(1986)016<0680:OTROIM>2.0.CO;2.

Vallis, G. K., 2000: Large-scale circulation and production of stratification: Effects of wind, geometry, and diffusion. *J. Phys. Oceanogr.,* **30,** 933–954, doi:10.1175/1520-0485(2000)030<0933:LSCAPO>2.0.CO;2.

Walin, G., 1982: On the relation between sea-surface heat flow and thermal circulation in the ocean. *Tellus,* **34A,** 187–195, doi:10.1111/j.2153-3490.1982.tb01806.x.

Wolfe, C. L., and P. Cessi, 2010: What sets the strength of the middepth stratification and overturning circulation in eddying ocean models? *J. Phys. Oceanogr.,* **40,** 1520–1538, doi:10.1175/2010JPO4393.1.

——, and ——, 2011: The adiabatic pole-to-pole overturning circulation. *J. Phys. Oceanogr.,* **41,** 1795–1810, doi:10.1175/2011JPO4570.1.

Wunsch, C., and R. Ferrari, 2004: Vertical mixing, energy, and the general circulation of the oceans. *Annu. Rev. Fluid Mech.,* **36,** 281–314, doi:10.1146/annurev.fluid.36.050802.122121.

Xie, P., and G. Vallis, 2012: The passive and active nature of ocean heat uptake in idealized climate change experiments. *Climate Dyn.,* **38,** 667–684, doi:10.1007/s00382-011-1063-8.

Zika, J. D., W. P. Sijp, and M. H. England, 2013: Vertical heat transport by ocean circulation and the role of mechanical and haline forcing. *J. Phys. Oceanogr.,* **43,** 2095–2112, doi:10.1175/JPO-D-12-0179.1.